22 Tetralogy of Fallot

Shubhika Srivastava[1] and Ira A. Parness[2]

[1]Echocardiography Laboratory, Mount Sinai Medical Center, New York, NY, USA
[2]Division of Pediatric Cardiology, Mount Sinai Medical Center, New York, NY, USA

Definition

In 1671, Niels Stenson first described the pathology of the syndrome now known as tetralogy of Fallot (TOF). Fallot, in his seminal paper, was careful to point out the previous work and published cases of the same syndrome. However, it was not until his 1888 paper that Etienne-Louis Arthur Fallot debunked the prevailing theory that cardiac cyanosis ("la maladie bleue") was due to right-to-left foramen ovale shunting. Fallot was the first to appreciate that most patients with cyanotic heart disease had the complex of cardiac malformations that he coined a "tetralogy" consisting of pulmonary stenosis, ventricular septal defect (VSD), dextroposition of the aorta, and right ventricular (RV) hypertrophy [1–3]. Fallot postulated that the tetralogy was the consequence of an intrauterine malformation of the subpulmonary infundibulum and the pulmonary valve [2], and Fallot's assessment was later adopted by Abbott and Dawson [4] who, in 1924, named the malformation "tetralogy of Fallot." The nomenclature for TOF as recommended by the Congenital Heart Surgeons Society, to unify reporting and for multiinstitutional studies, classified TOF into three main groups:

1 TOF with varying degrees of pulmonary stenosis
2 TOF with common atrioventricular (AV) canal
3 TOF with absent pulmonary valve.

TOF with pulmonary atresia was classified under the category of pulmonary atresia with VSD [5]. Nonetheless, in this chapter, we have categorized pulmonary atresia with VSD as the most severe morphologic variant of TOF.

Incidence

Tetralogy of Fallot is the most common cyanotic heart defect, with an incidence of 32.6 per 100 000 live births [6,7]. Early neonatal complete repair was pioneered by Castaneda and colleagues [8] and was aimed at minimizing the exposure to cyanosis, as well as minimizing RV hypertrophy and promoting alveologenesis [9]. Initial medical and surgical mortality in the 1980s was reported to be as high as 28% [10], and subsequent improvement in diagnostic, surgical and anesthetic techniques has had a significant impact on the natural history of repaired TOF. There is now a large population of adults with repaired TOF, which has necessitated advances in diagnostic techniques and management [11].

Embryology, genetics and molecular basis

The pathognomonic conotruncal abnormality of TOF has been attributed to arrest in neural crest cell migration [12]. Studies in chick and mouse embryos have demonstrated the key role of the secondary heart field (SHF) from the anterior mesoderm in cardiac embryogenesis [12–15], including a significant role in conotruncal and RV development in humans [16,17]. Following primary heart tube looping, committed precardiac cells from the SHF migrate to the anterior pole, where they are incorporated into the outflow tracts. Neural crest cells influence and modulate migration of the SHF. Ablation of the SHF and/or neural crest (NC) results in arrest of caudal migration of the committed precardiac cells toward the aortic sac [18–22]. The consequent short outflow tract [23], failure of normal rotation of the conotruncus, and abnormal coronary arteries are typical of TOF [24].

This embryologic theory supports the hypothesis proposed by Van Praagh and colleagues, who demonstrated that the primary morphologic abnormality in TOF is an underdeveloped subpulmonary infundibulum [3]. The secondary precardiac mesoderm expresses NKX2.5 and GATA 4 transcription factors [15,18,19]. Hence, gene defects affecting their expression may explain the resultant conotruncal abnormality in TOF. Microdeletion of chromosome 22q11, seen in DiGeorge or velocardiofacial phenotype syndromes, is a common example of a single gene defect causing

Echocardiography in Pediatric and Congenital Heart Disease: From Fetus to Adult
Edited by Wyman W. Lai, Luc L. Mertens, Meryl S. Cohen and Tal Geva
 ISBN: 978-1-405-17401-5

abnormal neural crest cell migration and resulting in TOF [17]. The prevalence of 22q11 deletions among patients with TOF is much higher in patients with associated pulmonary atresia than in patients with TOF alone [25].

The subpulmonary infundibulum derived from the SHF is highly sensitive to vascular endothelium growth factor (VEGF) signaling, which influences growth of the outflow tract cushions and RV myocardium. Hypoxia and other gene defects that cause upregulation of VEGF induce hyperplasia of the outflow tract cushions and apoptosis of the subpulmonary infundibulum. The resultant morphology is hypoplasia of the pulmonary trunk, right ventricular outflow tract (RVOT) obstruction and dextroposition of the aorta [26].

Approximately 50 syndromes associated with TOF have been identified [27]. Genetic syndromes have been shown to be an independent risk factor for mortality in TOF repair [28]. Known chromosomal anomalies, syndromes and single gene defects are associated with at least one-third of the cases with TOF (Table 22.1). In one study of 87 patients with TOF and associated common AV canal, 87.5% had a genetic syndrome and extracardiac abnormalities, 67% had Down syndrome, but none had 22q11 deletion [29].

Environmental factors

Maternal diabetes, exposure to retinoic acid, maternal phenylketonuria, and trimethadione have been reported to be associated with TOF [46–48].

Recurrence risk

The recurrence rate of TOF varies between 2.5% and 3% if one sibling is affected, and is 8% if more than one sibling is affected. The reported risk of recurrence is 1.4% from an affected father, and varies between 0.9% and 2.6% for an affected mother. The recurrence rate also depends upon associated syndromes and genetic or environmental factors [49–55].

Morphology

The conotruncus in TOF

Tetralogy of Fallot comprises conoventricular VSD, overriding aorta, RV outflow tract obstruction, and RV hypertrophy (Figs 22.1 and 22.2). However, the RV hypertrophy component is the consequence of prolonged systemic level RV pressures rather than being a primary morphologic feature. The principal developmental abnormality in TOF resulting in its components has been debated. There are two theories:

1 The theory advocated by Van Praagh and colleagues [2,3,56]: The principal morphologic abnormality in TOF is hypoplasia of the subpulmonary infundibulum, the latter consisting of the parietal band and the muscle or conus subtended under the pulmonary valve [3]. The combination of a small subpulmonary infundibulum, or conus (they are synonyms), and absence of subaortic conus results in the antero-cephalad deviation of the infundibular septum. According to Van Praagh, the normal aortic overriding of the ventricular septum is exaggerated by the presence of a VSD in TOF and by the dilated aorta. The relationship between the aortic valve and pulmonary valve in severe TOF is often altered, with significant clockwise rotation of the conotruncus resulting in a rightward and more anteriorly located aortic valve, and a leftward and more posteriorly situated hypoplastic pulmonary valve [3].

2 Becker et al. [1,57] and Anderson et al. [57,58], proposed that the principal abnormality in TOF is antero-superior deviation of the infundibular septum and not hypoplasia of the subpulmonary infundibulum. Because anterior deviation of

Table 22.1 Genetic syndromes associated with tetralogy of Fallot (TOF)

Anomaly	Known prevalence in TOF	Gene defect	Chromosome location	References
Trisomy 21	8% (14% in fetal series)	Not identified		[27,30,31]
Trisomy 13	7% in fetal series			[31]
Trisomy 18	16%			[32]
Velocardiofacial	20% (80% of those with RAA)	*TBX1* in 15%	22q11	[27]
Noonan	Rare	*PTNPII*, *KRAS*, *SOS1*	12q24	[33–36]
Alagille	16%	*JAG1*	20p12	[37,38]
Holt–Oram	Rare	*TBX5*		[39]
Goldenhar, or oculoauriculovertebral syndrome	10%			[40]
DiGeorge	8–35%		90% have 22q11	[41–44]
Cardiac homeobox gene mutations	4%	*NKX2.5*	5q34-q35	[5,27,42]
	?	*ZFPM2/FOG2*	8q23	[17,24,45]
Cat-eye	Rare		Duplication of 22pter22q11	[27]

RAA, right aortic arch.

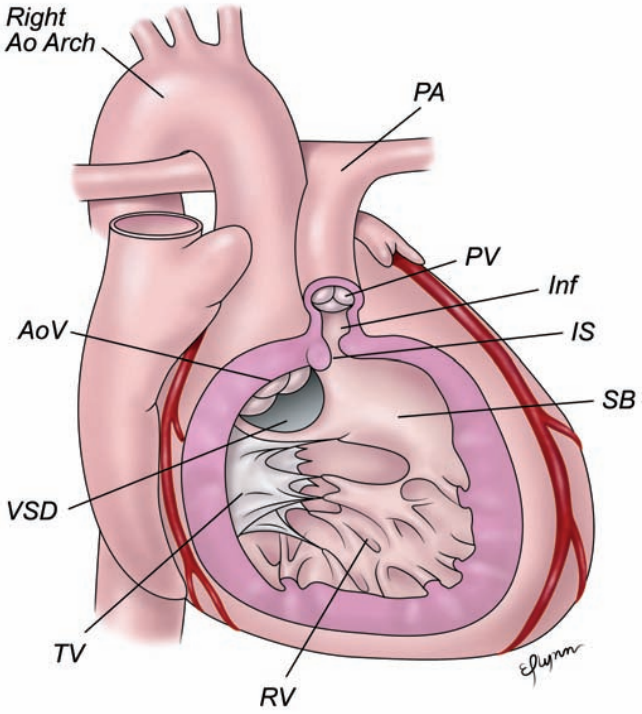

(a)

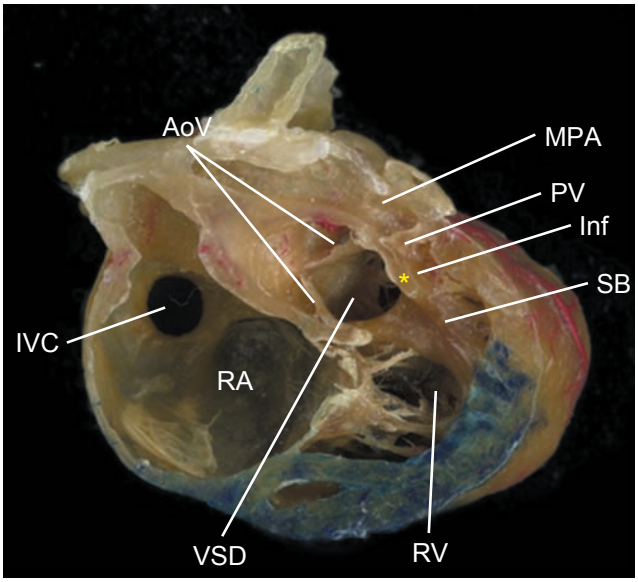

(b)

Figure 22.1 Tetralogy of Fallot (TOF) with pulmonary stenosis. **(a)** Diagram showing anterior-leftward deviation of the infundibular septum (IS) relative to the muscular ventricular septum, narrowed subpulmonary infundibulum (Inf), pulmonary valve (PV) stenosis, right ventricular (RV) hypertrophy, aortic override, and right aortic arch. The ventricular septal defect (VSD) is enclosed anteriorly and postero-inferiorly between the limbs of the septal band (SB) and superiorly by infundibular septum and the junction of the anterior limb of septal band and RV free wall. This anterior malalignment type of conoventricular septal defect is typical of TOF. **(b)** Waxed heart specimen showing the right side of the heart of an infant TOF with pulmonary stenosis. Courtesy of Dr Paul Weinberg, Children's Hospital of Philadelphia. AoV, aortic valve; IVC, inferior vena cava; MPA, main pulmonary artery; PA, pulmonary artery; RA, right atrium; TV, tricuspid valve; asterisk (*) denotes the infundibular septum.

the conal septum may be present without RV outflow obstruction as in Eisenmenger type VSD [59–61], there must also be concomitant hypertrophy and/or hypoplasia of the subpulmonary infundibulum to produce TOF morphology. The infundibular septal deviation theory also does not easily explain the morphologic variant of TOF with doubly committed subarterial VSD, characterized by complete absence of the conal septum but hypoplasia of the pulmonary valve.

In either scheme, the embryonic morphologic abnormality of conal hypoplasia and/or conal septal malalignment results in failure of ventricular septation (VSD), subpulmonary and/or valvar pulmonary stenosis, and overriding of the aorta.

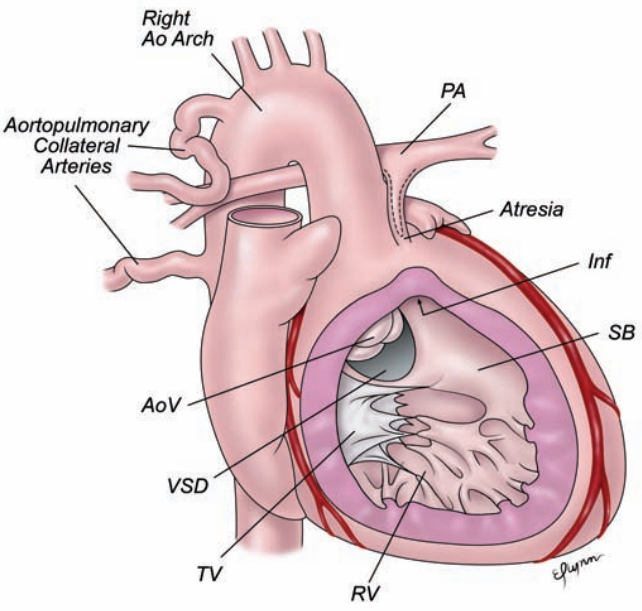

Figure 22.2 (*left*) Diagram of tetralogy of Fallot (TOF) with pulmonary atresia. The subpulmonary infundibulum is obliterated by marked anterior-leftward malalignment of the conal septum. The pulmonary arteries are hypoplastic and aorto-pulmonary collateral vessels are shown. The anterior malalignment type of conoventricular septal defect is the same as in TOF with pulmonary stenosis. AoV, aortic valve; Inf, infundibulum; IVC, inferior vena cava; MPA, main pulmonary artery; PA, pulmonary artery; RV, right ventricle; SB, septal band; TV, tricuspid valve; VSD, ventricular septal defect.

Ventricular septal defect morphology

The anterior malalignment type of conoventricular septal defect is typical of TOF (Fig. 22.1) [2,62]. Some authors have classified these defects as paramembranous or perimembranous [63]. The defect results from anterior, superior

and leftward deviation of the conal (infundibular or outlet) septum, which fails to align with the crest of the muscular septum. The malalignment of conal septum results in a wide communicating space between the ventricles rather than a deficiency, per se, in the "pars membranacea." The boundaries of the defect are formed by:

- Superiorly – the RV free wall and the aortic valve cusps, extending posteriorly to the tricuspid valve hinge point.
- Anteriorly – the parietal band of the crista supraventricularis.
- Inferiorly – the crest of the ventricular septum.
- Posteriorly – the muscle extending from septal band to the posterior muscular septum, also called the posterior limb of septal band. This muscle also separates the aortic valve from the tricuspid valve and is often referred to as the ventricular infundibular fold, which forms the inner heart curvature in a structurally normal heart. The width of this muscle is variable, at times being represented as a thin fibrous ridge allowing approximation of the tricuspid valve to the VSD [63].

The VSD is thus enclosed anteriorly and postero-inferiorly between the limbs of the septal band, and superiorly by the conal septum and the junction of the anterior limb of septal band and RV free wall [57]. Absence of the conal septum and associated hypoplasia of the subpulmonary infundibulum and hypertrophy of the septoparietal band results in a variant of TOF with doubly committed subarterial VSD, overriding aorta, and pulmonary annular hypoplasia and stenosis [64–67].

The VSD in TOF is typically large but a restrictive defect has been reported in 1.5% of cases [68,69]. The mechanism of obstruction in nearly all the cases results from overlying abnormal or accessory tissue associated with the tricuspid valve [69–72]. Rarely, myxomatous outpouching of the septal leaflet associated with Ebstein anomaly in TOF can result in a restrictive VSD [73]. Absolute small dimensions of the VSD caused by posterior deviation of the septal band and hypertrophy of the ventricular septum resulting in restriction to flow have rarely been described [68].

Tetralogy of Fallot can also be seen in association with common AV canal defects [57,74] characterized by an anteriorly malaligned conal septum in association with a predominantly Ratelli type C common AV valve [75]. In the setting of complete common AV canal and TOF, VSD morphology is that of a single defect with confluent inlet and outlet components along with the typically anteriorly deviated conal septum. TOF may also occur in association with a rare variant of common AV canal in which there is an absent or diminutive atrial septal defect component [76].

Coronary arteries

Clockwise rotation of the aortic root (as viewed from the cardiac apex), and resultant rotated origins of the coronary arteries, are typical in TOF. Anomalies in the branching pattern of the coronary arteries are reported in approximately 5% of all cases (Fig. 22.3) [77]. The most common anomaly, occurring in 3%, is origin of the left anterior descending (LAD) coronary artery from the right coronary artery (RCA); this is followed by dual LAD in 1.8%, single RCA in 0.3%, single left coronary artery (LCA) in 0.2%, and coronary-to-pulmonary artery fistula in 0.2%. In an angiographic study, anomalies of coronary artery branching pattern were more prevalent in patients with the most prominent aorto-pulmonary rotation [78]. The extraordinarily rare "isolated infundibuloarterial inversion" in TOF is associated with the RCA crossing anteriorly across the subpulmonary infundibulum. Anomalous origin of the LCA from the pulmonary artery has been reported in patients with TOF [77, 79–82].

Coronary artery-to-pulmonary artery fistulae may rarely serve as a source of pulmonary blood flow in TOF with pulmonary valvar atresia or severe stenosis [83–85]. Isolated coronary ostial stenosis or obstruction has also been reported in the absence of any other coronary anomaly [81]. Acquired coronary cameral fistulae may be observed following surgery [86].

Variants and associated lesions

TOF and double-outlet right ventricle (DORV)

Some authorities have categorized extreme dextroposition or aortic overriding with more than 50% of the aortic annulus over the RV as DORV [57,58]. Nonetheless, according to Van Praagh et al., the maintenance of aortic-to-mitral valve fibrous continuity or normally related great arteries is pathognomonic for TOF irrespective of the degree of aortic override or dextroposition [2,57,87,88]. This approach recognizes a wide spectrum of aortic overriding within TOF without imposing an arbitrary dichotomous cutoff between TOF and DORV depending on the percentage of aortic override. Aortic–mitral fibrous continuity is also important in the prediction of postoperative left ventricular (LV) outflow tract obstruction: progressive subaortic obstruction following repair of typical TOF is rare [89]. However, progressive muscular hypertrophy causing subaortic obstruction may develop in cases of "TOF-like" DORV with retention of subaortic conus (see Chapter 25).

TOF and double-chambered right ventricle (DCRV)

Double-chambered right ventricle is an anomaly characterized by obstruction within the RV with or without an associated VSD (see Chapter 16). It can also present as a progressive lesion following corrective surgery for TOF [90]. DCRV is often misdiagnosed as TOF because both lesions have a VSD and subpulmonary stenosis [90–96]. However, in DCRV, the primary morphologic abnormality resulting in subpulmonary stenosis is either marked hypertrophy of the septoparietal trabeculations or moderator band, and/or abnormal displacement of the moderator band resulting in narrowing of the proximal infundibular ostium. Unlike TOF, DCRV is typically associated with normal size and morphology of the pulmonary valve and main and branch pulmonary arteries. Additionally, the VSD seen in DCRV is typically

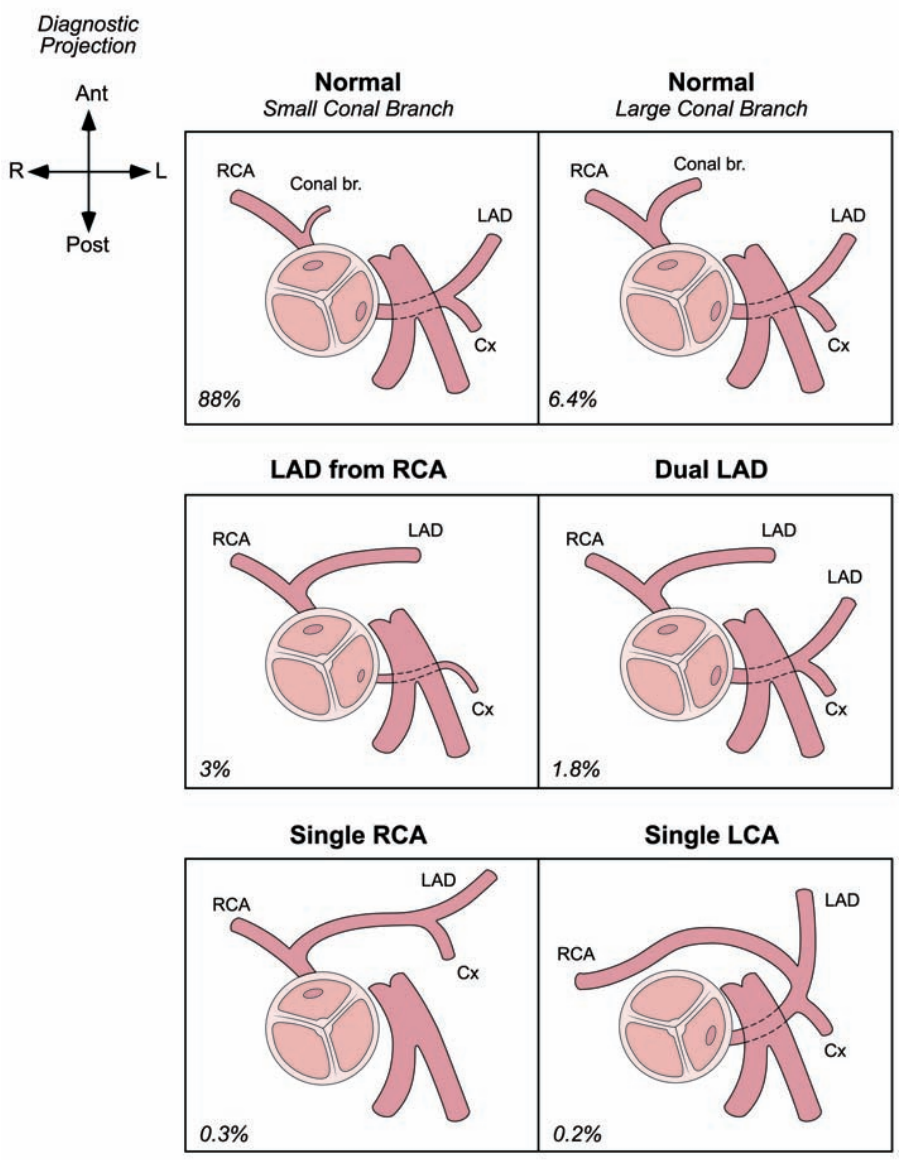

Figure 22.3 Diagram of coronary artery patterns in tetralogy of Fallot. br., branch; Cx, circumflex artery; LAD, left anterior descending coronary artery; LCA, left coronary artery; RCA, right coronary artery.

membranous rather than the malalignment type typical of TOF. However, there are overlap syndromes that share features of DCRV and TOF, such as those with an anterior malalignment type of VSD and aortic overriding but with a morphologically normal pulmonary valve and a well-developed infundibulum; in these cases, the subpulmonary obstruction is limited to the proximal os infundibulum.

TOF with pulmonary atresia and/or extreme pulmonary hypoplasia

Tetralogy of Fallot with pulmonary atresia is a severe form of TOF. In addition to valvar atresia (short-segment atresia) or valve and main pulmonary artery absence (long-segment atresia), this condition is characterized by marked variability in the degree of pulmonary artery hypoplasia or absence and/or the presence of abnormal pulmonary arterial supply. The intracardiac anatomy, like other forms of TOF, typically consists of an enlarged and overriding aorta and an anterior malalignment VSD. In addition, there is marked infundibular hypoplasia or subvalvar atresia due to extreme leftward deviation of the conal septum, which may merge with the septal parietal band and RV free wall.

This defect was initially misclassified as truncus arteriosus type IV in the classification of Collett and Edwards [97]. However, Van Praagh and Van Praagh correctly defined and classified this entity as TOF with pulmonary atresia [98]. This entity was also described as "pseudotruncus" by Bharati et al. [99]. The Congenital Heart Surgeons Society Nomenclature Committee classified TOF with pulmonary atresia under the umbrella of "Pulmonary atresia with VSD" [100]. The term "MAPCA(s)," or major aortopulmonary collateral artery, was coined by Macartney et al. [101].

Tetralogy of Fallot with pulmonary atresia can be further classified into three broad categories [100]:

1 Native confluent branch pulmonary arteries are present, which supply all lung segments; patency of the ductus maintains pulmonary circulation. Interruption of antegrade pulmonary blood flow may be limited to the level of the valve, as in valvar atresia, or to the main pulmonary artery, as in long-segment pulmonary atresia.

2 Both native pulmonary arteries and MAPCAs are present; lung segments can have dual blood supply and the native pulmonary arteries may be supplied by either a ductus and/or MAPCAs. The pulmonary atresia may be long-segment with confluent mediastinal branch pulmonary arteries or with discontinuous branch pulmonary arteries.

3 Native mediastinal pulmonary arteries are absent and MAPCAs supply all lung segments. Bronchial and pleural vessels can also be alternative sources of pulmonary blood flow.

The size of the branch pulmonary arteries is inversely proportional to the extent of MAPCAs and presence of a ductus arteriosus [102–105]. The angiographically determined Nakata index predicts good outcomes of complete repair of TOF with pulmonary artery hypoplasia if the index is greater than 100 mm^2/body surface area (BSA) [106].

Other rare variations in the morphology of TOF with pulmonary atresia have been reported, such as restrictive VSD (68,107,108), coronary artery-to-pulmonary artery fistula [75], aortopulmonary window [109], retroaortic innominate vein [110], and a higher incidence of right aortic arch [99,111].

TOF with atrioventricular canal defects

A common AV canal in association with TOF is a rare variant, seen in 1.7% of all cases of TOF and in 6.2% of cases with complete common AV canal defects [74,75]. A very high incidence (87.5%) of genetic and extracardiac abnormalities is seen in this morphologic variant [67].

Rastelli type C morphology of the common AV valve is the most common variant (85% of reported cases) [74]. The diagnosis of type A common AV valve morphology in TOF has been questioned by Suzuki et al., who argued that attachments of the superior bridging leaflet to the crest of a malalignment VSD are unlikely [75]. We have observed concomitant absence of conal septum in the setting of otherwise typical morphology for TOF with common atrioventricular canal (CAVC). A small or absent primum ASD component can also occur in this morphologic variant, which can increase the challenge of surgical correction of this lesion [74,112]. TOF may also exist in conjunction with a cleft mitral valve but with absent primum ASD [113].

TOF with absent pulmonary valve syndrome

The incidence of TOF with absent pulmonary valve is reported to be between 3% and 6% of all TOF [88,114,115]. This TOF variant with typical anterior malalignment VSD and overriding aorta is differentiated by hypoplasia of the pulmonary valve annulus with rudimentary valve leaflets causing pulmonary stenosis and insufficiency. The main and/or one or both branch pulmonary arteries are typically aneurysmally enlarged [116,117]. This lesion is usually associated with absent patent ductus arteriosus, and prenatal absence of the ductus arteriosus has been demonstrated by fetal echocardiography [116,118]. Aneurysmal pulmonary artery dilation is associated with variable degrees of bronchial compression and intraparenchymal pulmonary arteriopathy, and may cause severe neonatal respiratory distress. In fetal life, severe forms may lead to hydrops fetalis and/or fetal demise.

Aortic arch anomalies

Right aortic arch (RAA) is seen in approximately 25% of patients with TOF [119,120]. Double aortic arch and persistence of the fifth aortic arch and other morphologic variations of vascular rings may be seen in association with TOF [101, 121,122].

Right aortic arch with isolation of the subclavian artery or with aberrant origin of the left subclavian artery from the ascending aorta have been reported [123,124]. The isolated left subclavian artery can be supplied by the left vertebral artery (in which case the direction of blood flow is reversed) and may cause a subclavian steal phenomenon. Alternatively, the isolated left subclavian artery may be connected via a patent ductus arteriosus to the main pulmonary artery. In the latter case, the left vertebral artery supplies the main pulmonary artery resulting in a congenital pulmonary artery steal [123,125,126].

Aortopulmonary defects and variations in pulmonary artery origin and bifurcation

Aortic origin of branch pulmonary artery [127,128], unilateral absence of branch pulmonary artery, crossed pulmonary arteries [80,129], aortopulmonary window [109,130,131], and pulmonary artery slings [132,133] have been described in association with TOF. Crossed pulmonary arteries may be a marker for 22q11 deletion [129,134–136].

Left-sided lesions associated with TOF

Isolated reports of supravalvular mitral stenosis, LV outflow tract obstruction secondary to adherent anterior mitral valve leaflet, and cleft mitral valve have been described in patients with TOF [62,113,137]. Other left heart lesions reported in association with TOF include aortic valve abnormalities (bicommissural, stenosis, regurgitation) [138–141], coarctation of the aorta [139], LV diverticulum [142], and cor triatriatum [143,144].

Rare segmental combinations in TOF

The usual segmental anatomy of TOF is {S,D,S}, with the rare occurrence of {I,L,I} in dextrocardia, the latter being

sometimes seen in association with the "polysplenia" type of heterotaxy syndrome [145]. Isolated infundibuloarterial inversion in the setting of atrial situs solitus, D-looped ventricles, and inversus normally related great arteries or {S,D,I} has been reported in TOF [146–148]. The presence of aortic-to-mitral valve fibrous continuity differentiates this rare conotruncus from that of anatomically corrected malposition.

Systemic and pulmonary venous anomalies and atrial septal defects

In TOF, systemic and pulmonary venous anomalies may be seen independently or in association with heterotaxy syndrome [149–151]. Subaortic (retroaortic) position of the innominate vein is more commonly seen in TOF with pulmonary atresia [110]. Left superior vena cava to the coronary sinus (or rarely, to the left atrium) has been described in up to 11% of cases [114,152]. Left superior vena cava to left atrium without a connecting left innominate vein, if undiagnosed, can result in persistent hypoxemia following complete repair. Persistence of the levoatrial cardinal vein has also been reported [151]. Partially or totally anomalous pulmonary venous connection may be seen in association with TOF [153], rarely as part of scimitar syndrome [154]. Atrial septal defects, typically secundum type, are seen in 86% of cases [114]. Rarely, sinus venosus defects or coronary sinus septal defects occur in TOF [150,155].

Other rare associated malformations

Ebstein anomaly and double-orifice tricuspid valve (TV) have been reported in TOF [73,156]. The association of TOF with ectopia cordis (often in combination with other midline defects and ventricular diverticulum) is known as "pentalogy of Cantrell" [157].

Imaging

Detailed echocardiographic assessment has made diagnostic angiography nearly obsolete in the routine preoperative assessment of the anatomic details of TOF. However, angiography and cardiac magnetic resonance (CMR) serve an important complementary role in the assessment of rare aortic arch anomalies as well as MAPCAs and hypoplastic branch pulmonary arteries in the setting of associated pulmonary atresia and in absent pulmonary valve syndrome. CMR provides unique information about pulmonary vessels *and* airway architecture, both of which are important for surgical planning.

Preoperative echocardiographic assessment of morphology

The goals of preoperative assessment can be summarized as follows:

- Cardiac position and presence or absence of thymus.
- Visceral and atrial situs and segmental diagnosis; conotruncal anatomy.
- Pulmonary and systemic venous connections and atrial septal defects.
- AV valve morphology and function.
- VSD morphology, differentiating between malalignment, doubly committed subarterial, and AV canal types [158]. Rule out additional muscular ventricular septal defects. Assess for rare restriction to flow and determine the direction of VSD shunting.
- Degree and morphology of RV outflow obstruction: assess infundibular septal size and position as well as additional muscular obstruction, as in DCRV.
- Assess pulmonary valve annular size and valve morphology.
- Determine main and branch pulmonary artery size and flow. Rule out anomalous origin or course of branch pulmonary arteries (e.g., left pulmonary artery [LPA] sling). Evaluate for branch pulmonary artery hypoplasia, discrete branch pulmonary artery stenosis, or discontinuous branch pulmonary arteries, especially following ductal closure.
- Subaortic and aortic valve morphology and function.
- Image PDA origin from the aortic arch or from the brachiocephalic arteries and rule out additional sources of pulmonary blood flow such as aorto-pulmonary collaterals. Distinguish PDA from MAPCA.
- Determine aortic arch sidedness and branching pattern. Assess for vascular rings and other arch malformations.
- Image coronary artery origin, branching, and flow; rule out anomalous origin of the LCA from the main pulmonary artery; anomalous origin of the LAD from the RCA or other large coronary branches crossing the RV outflow tract that may complicate transannular patch repair or conduit placement.

Anatomic two-dimensional assessment

Organized, systematic, and detailed imaging starting with the subxiphoid long-axis window is our preferred approach for accurate diagnosis of congenital heart disease (see Chapter 4). At Mount Sinai Medical Center in New York, we routinely sedate infants with congenital heart disease using chloral hydrate. However, in TOF with moderate stenosis, sedation imposes an additional risk for a hypercyanotic spell due to the combination of intravascular volume depletion (from being kept NPO [nil per os] for sedation) and systemic vasodilation. Hence, whenever possible we aim at defining the details of branch pulmonary artery anatomy, arch morphology and coronary morphology early after diagnosis in the newborn period. Neonates will often sleep soundly after feeding, allowing a comprehensive and detailed examination without sedation.

Initial subxiphoid long-axis imaging

This view demonstrates visceral and atrial situs, systemic venous connections, coronary sinus and atrial septal morphology [159] (Videoclip 22.1). The descending aorta in

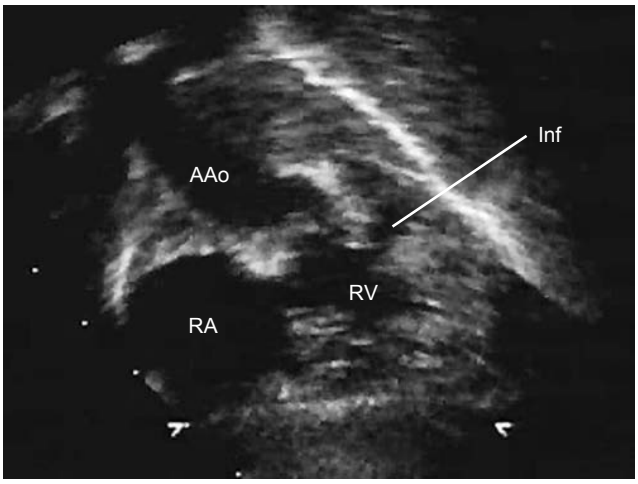

Figure 22.4 Imaging of tetralogy of Fallot with pulmonary stenosis from the subxiphoid long-axis view. Anterior tilt of the transducer demonstrates the infundibular stenosis (Inf) and the ascending aorta (AAo). RA, right atrium; RV, right ventricle.

its cross-section may be visualized to the left of the spine, and through the course of the sweep it can be seen crossing over to the right of the thoracic spine. The VSD with overriding of the aorta may be seen as well as subpulmonary infundibular hypoplasia and stenosis (Fig. 22.4). Branch pulmonary arteries may also be identified from subxiphoid long-axis imaging (Fig. 22.5; Videoclip 22.2) as the RPA traverses from left to right above the atrial mass; the LPA and ductus are more difficult to image without color Doppler flow mapping.

Subxiphoid short-axis imaging

This view defines the atrial septum, the entrance of the right upper pulmonary vein into the left atrium, VSD, RV hypertrophy, and muscle bundles within the RV that could result in additional intracavitary obstruction, as in the DCRV variant (Fig. 22.6). Cleft mitral valve and common AV valve are also well imaged in this plane (Fig. 22.7 and Videoclip 22.3).

Anterior oblique subxiphoid view

This modified view is of exceptional benefit in viewing the subpulmonary infundibulum, inclusive of both the size of the conal septum and its displacement (Fig. 22.8 and Videoclip 22.4) [160]. This view is also useful for assessing additional muscle bundles contributing to RV outflow tract obstruction in the DCRV variant.

Apical views

Apical views demonstrate the AV valves, VSD, aortic valve (Fig. 22.9 and Videoclip 22.5), and may identify other associated anomalies, such as left-sided obstructive lesions.

Parasternal long-axis imaging

Parasternal imaging may be limited if the thymus, which usually provides a reliably good acoustic window, is absent. This view nicely demonstrates the overriding aorta, aortic-to-mitral valve fibrous continuity (distinguishing TOF from its related type of DORV) (Fig. 22.10a), VSD morphology, and pulmonary valve morphology as the transducer sweeps leftward and anteriorly (Fig. 22.10b and Videoclip 22.6).

Parasternal short-axis imaging

This view further defines VSD morphology, subpulmonary obstruction, infundibular hypertrophy, and deviation of the conal septum (Fig. 22.11 and Videoclip 22.7). Extension of the edge of the VSD beyond the intercoronary commissure under the right and noncoronary cusps and bordering the pulmonary valve annulus in the absence of the conal septum defines a doubly committed subarterial defect in TOF [66].

(a)

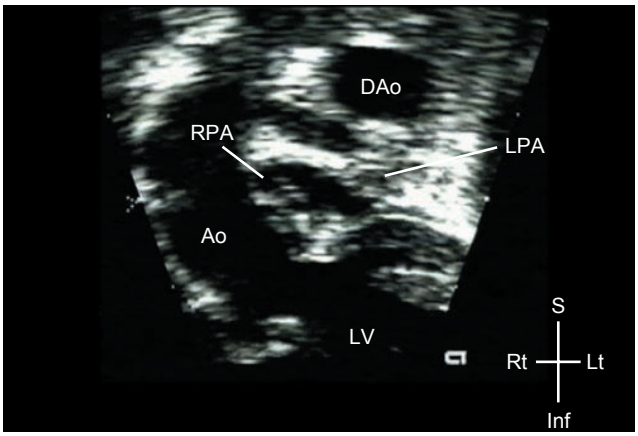

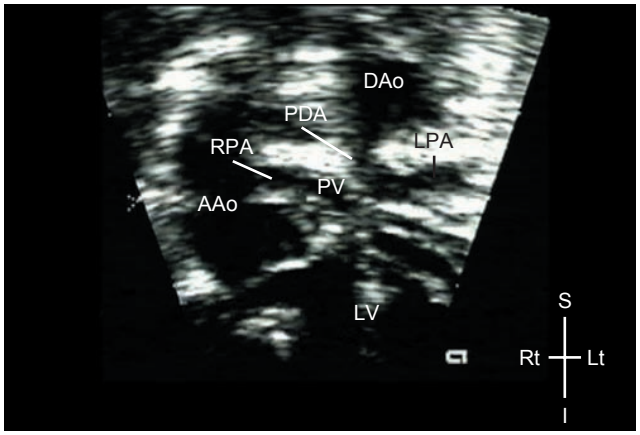

(b)

Figure 22.5 Imaging branch pulmonary arteries from the subxiphoid long-axis view in tetralogy of Fallot. **(a)** Hypoplastic, continuous branch pulmonary arteries. **(b)** Discontinuous branch pulmonary arteries. The right pulmonary artery (RPA) is continuous with the main pulmonary artery, and the discontinuous left pulmonary artery (LPA) is supplied by a patent ductus arteriosus (PDA). AAo, ascending aorta; DAo, descending aorta; LV, left ventricle; PV, pulmonary valve; S, superior; I, inferior; Rt, right; Lt, left.

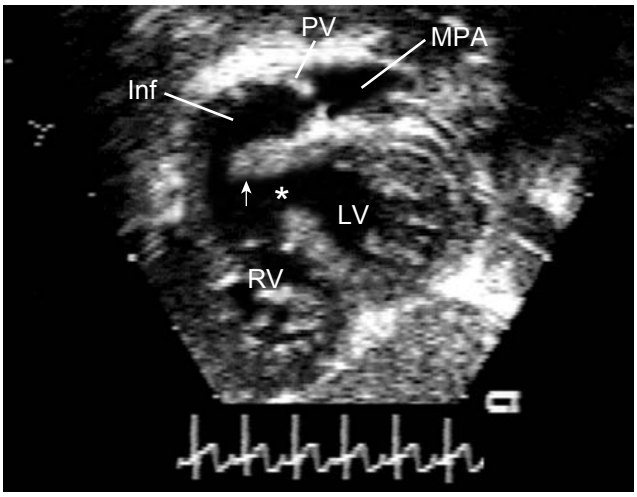

Figure 22.6 Subxiphoid short-axis view in tetralogy of Fallot showing anterior-superior malalignment of the infundibular septum (arrow) resulting in infundibular stenosis. The anterior malalignment type of conoventricular septal defect (*) is bordered superiorly by the infundibular septum (arrow) and inferiorly by the muscular ventricular septum. Inf, infundibulum; LV, left ventricle; MPA, main pulmonary artery; PV, pulmonary valve; RV, right ventricle.

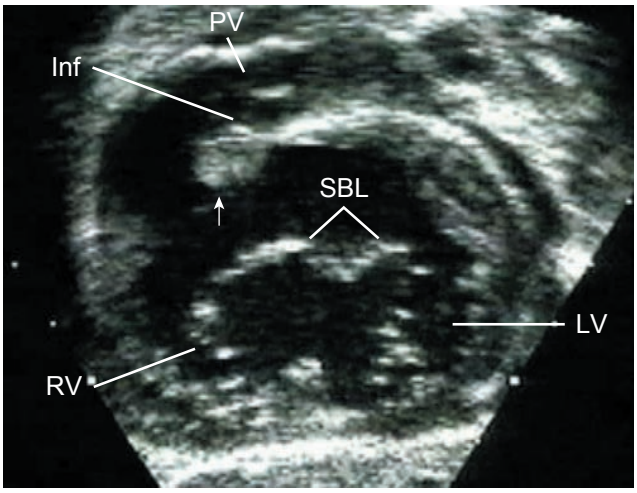

Figure 22.7 Subxiphoid short-axis view showing tetralogy of Fallot with complete common atrioventricular (AV) canal defect. Note the undivided and unattached superior bridging leaflet (SBL), consistent with Rastelli type C morphology of the superior leaflet. The conal septum (arrow) is deviated anteriorly and superiorly and the subpulmonary infundibulum (Inf) is small. The conoventricular septal defect is confluent with AV canal (inlet) ventricular septal defect. LV, left ventricle; PV, pulmonary valve; RV, right ventricle.

Imaging of the coronary arteries

The operator should employ the highest frequency transducers that will penetrate to achieve high-resolution coronary artery imaging. The Nyquist limit should be lowered on Doppler interrogation to accentuate low-velocity flow.

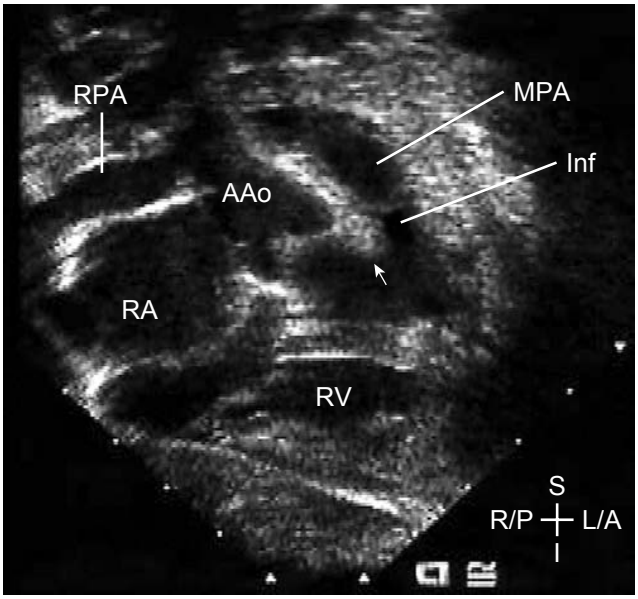

Figure 22.8 Subxiphoid oblique coronal view demonstrating the anterior deviated infundibular septum (arrow), narrowed subpulmonary infundibulum (Inf), and main pulmonary artery (MPA). AAo, ascending aorta; RA, right atrium; RV, right ventricle; RPA, right pulmonary artery; S, superior; I, inferior; L/A, left-anterior; R/P, right-posterior.

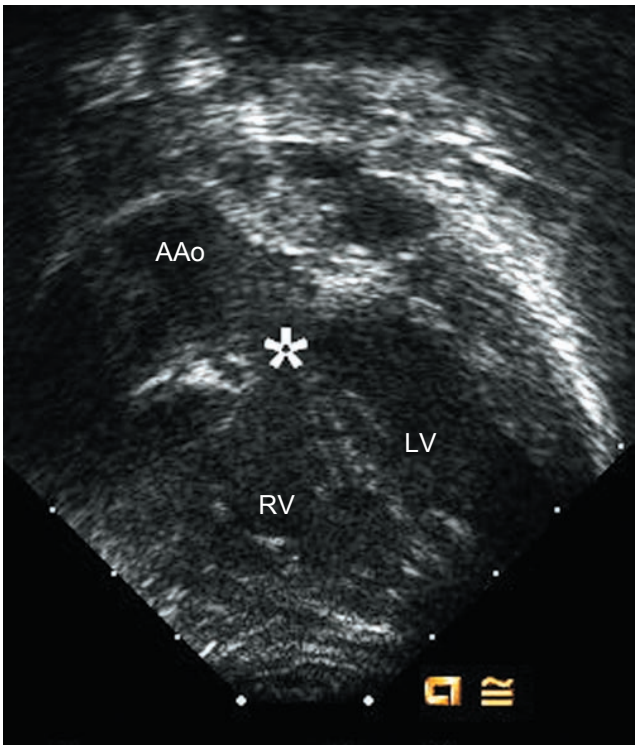

Figure 22.9 Anteriorly angled apical view showing the ventricular septal defect (*) and the overriding aorta (AAo). LV, left ventricle; RV, right ventricle.

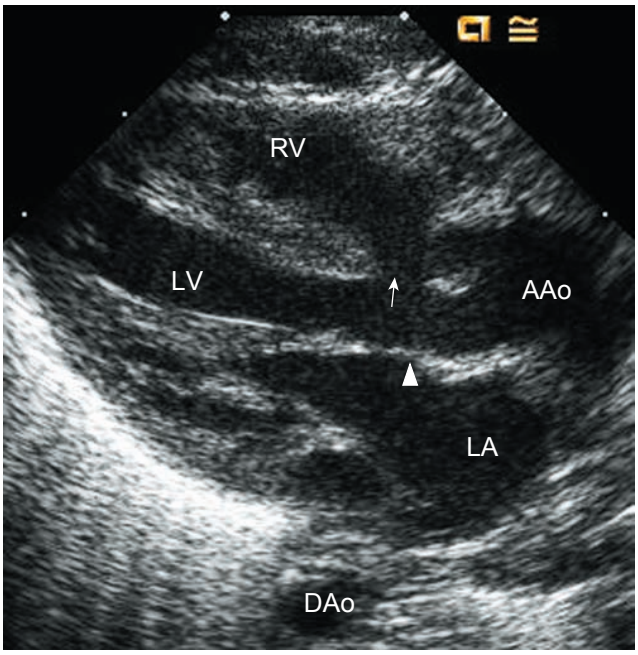

(a)

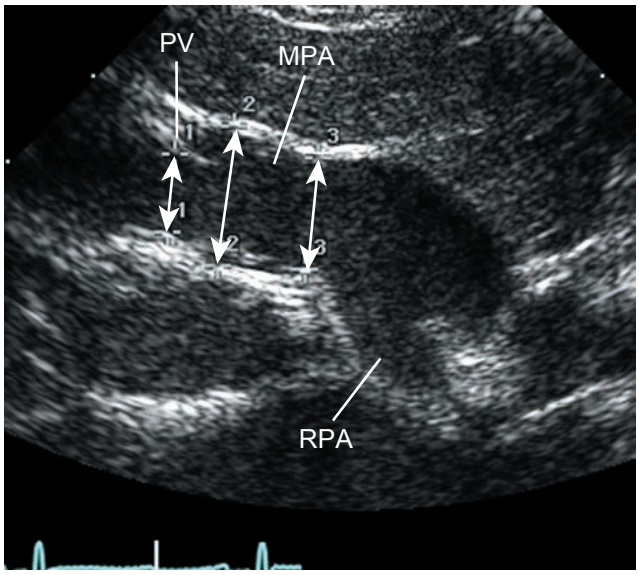

(b)

Figure 22.10 Parasternal long-axis view. **(a)** Image of the large conoventricular septal defect (arrow) with the aortic valve overriding the ventricular septum. Note the fibrous continuity between the aortic and mitral valve (arrowhead). **(b)** Tilting the transducer toward the left shoulder demonstrates the pulmonary valve (PV), main pulmonary artery (MPA) and proximal right pulmonary artery (RPA). Measurements of the pulmonary valve annulus and MPA are shown. AAo, ascending aorta; DAo, descending aorta; LA, left atrium; LV, left ventricle; RV, right ventricle.

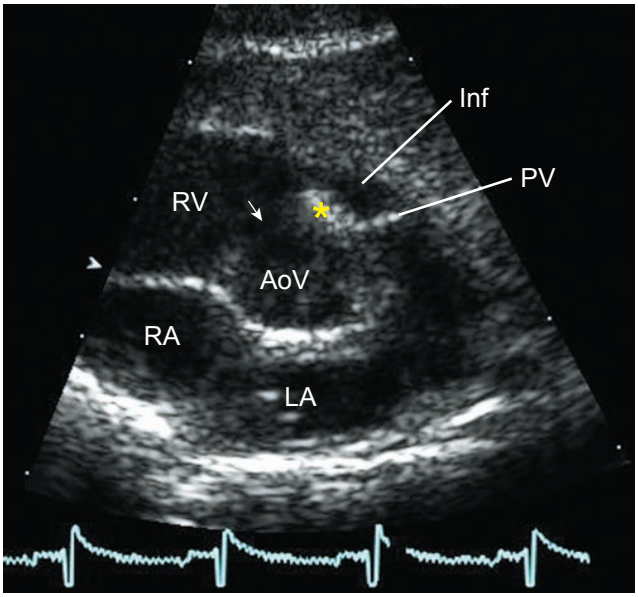

Figure 22.11 Parasternal short-axis view showing anterior deviation of conal septum (*) and a hypoplastic infundibulum (Inf) with severe subpulmonary narrowing. The ventricular septal defect is clearly seen in this view (arrow). AoV, aortic valve; LA, left atrium; PV, pulmonary valve; RA, right atrium; RV, right ventricle.

The origin of the coronary arteries can be demonstrated from the short-axis image. Clockwise rotation of the origins as viewed from the apex, a common finding in TOF, may be appreciated in this view. The left main coronary artery and its bifurcation are elongated by clockwise rotation of the transducer from the short axis into a transverse plane. Evaluation for a LAD coronary artery origin from the RCA crossing the RV outflow tract requires a careful sweep from the standard reference view in the parasternal long axis, angling toward the left shoulder (Fig. 22.12). Additional views that may be helpful include a high left parasternal cut in a transverse plane (Videoclip 22.8) or a modified apical 4-chamber view angled anteriorly; the latter aims at "shaving" the anterior wall of the RV outflow tract. Prominent crossing conal branches or dual LAD may be diagnosed in these sweeps, or occasionally from the most coronal extent of subxiphoid long-axis sweeps. Rare single RCA or LCA and anomalous origin of the LCA from the pulmonary artery may also be diagnosed. However, the echocardiographer must recognize that the turbulent pulmonary artery flow jets that characterize TOF may obscure the retrograde coronary flow emptying into the pulmonary artery.

Ductal views

Imaging is best performed from a high parasternal window in a parasagittal plane and/or from the suprasternal notch long-axis view. At times, differentiating between a ductus and aorto-pulmonary collateral is difficult because both may arise from the same location in the proximal descending thoracic aorta. However, the termination of the vessel at the proximal branch pulmonary artery origin is consistent with a ductus arteriosus, whereas aorto-pulmonary collaterals usually insert more distally into the branch pulmonary arteries

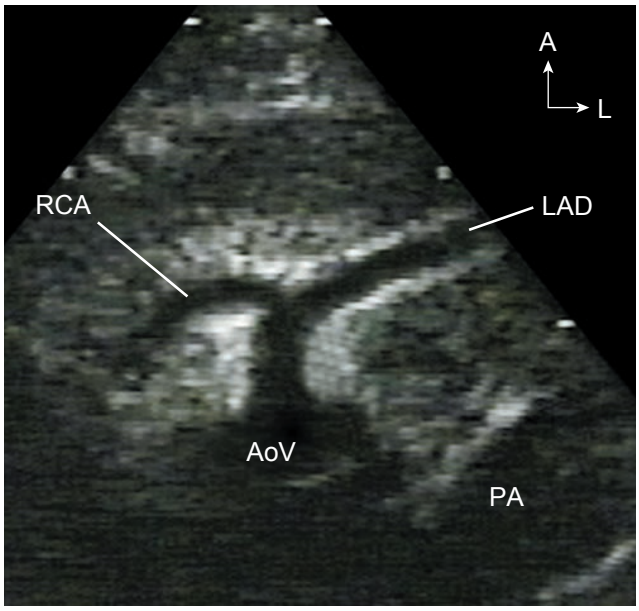

(a)

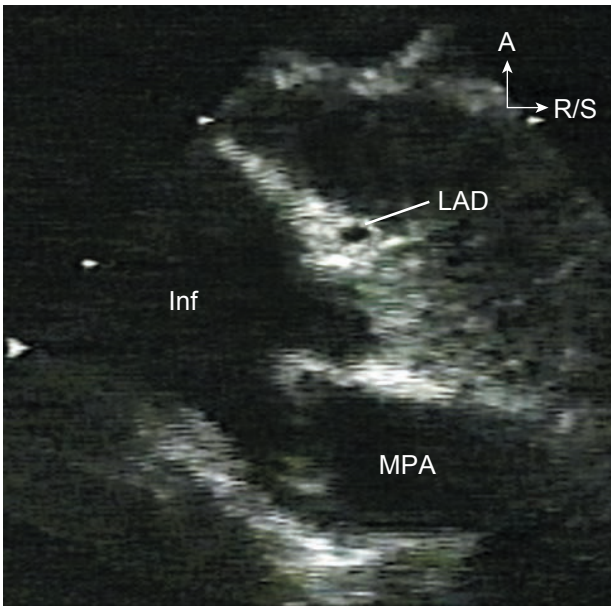

(b)

Figure 22.12 Anomalous origin of the left anterior descending (LAD) coronary artery from the right coronary artery (RCA) in an infant with tetralogy of Fallot. **(a)** Modified parasternal short-axis view showing a prominent RCA arising from the right aortic sinus of Valsalva, which is rotated clockwise. The LAD arises from the proximal RCA and traverses the infundibular free wall. **(b)** Parasternal long-axis view with the transducer tilted toward the left shoulder demonstrates the LAD in cross-section in the infundibular free wall. AoV, aortic valve; Inf, infundibulum; MPA, main pulmonary artery; A, anterior; L, left; R/S, right-superior.

near the hilum. Additionally, orthogonal imaging in a coronal plane from a high left parasternal view will demonstrate the site of ductal insertion into the proximal branch pulmonary artery to evaluate the possibility for development of peripheral pulmonary artery stenosis or discontinuity consequent to ductal closure. Crossed pulmonary arteries are diagnosed when the RPA originates inferiorly from the left aspect of MPA and the LPA originates more superiorly from the right aspect of MPA.

High left parasternal imaging

This view helps to evaluate the main and branch pulmonary arteries (Figs 22.13 and 22.14; Videoclip 22.9). It is important to align the beam perpendicularly to the pulmonary artery being interrogated by altering the window of interrogation for each pulmonary artery. High (subclavicular) left sternal border windows are best for the main and left pulmonary arteries. High (subclavicular) right sternal border windows are best for the RPA. Larger branch pulmonary arteries have a lesser likelihood of concomitant presence of aorto-pulmonary collaterals. A branch pulmonary artery diameter z-score of less than –2.5 had a sensitivity of 88% and specificity of 100% for the presence of one or more MAPCAs [103].

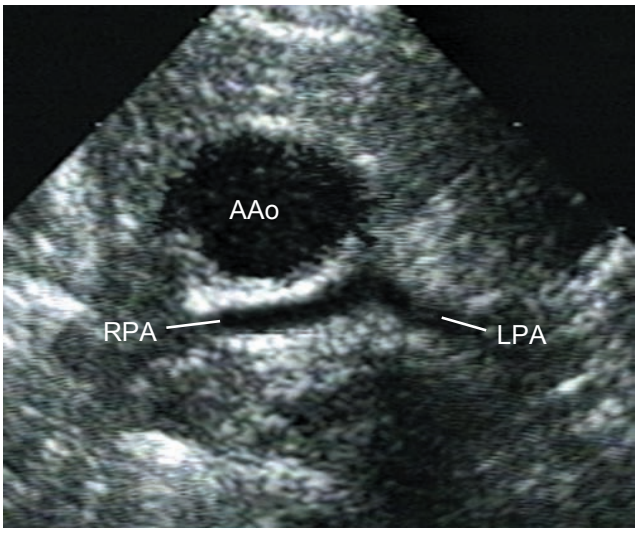

Figure 22.13 Imaging of the branch pulmonary arteries from the high left parasternal window in an infant with tetralogy of Fallot and pulmonary atresia. Note the confluent, hypoplastic left (LPA) and right (RPA) pulmonary arteries. AAo, ascending aorta.

Suprasternal notch imaging

Arch sidedness and branching pattern, retroaortic innominate vein (Fig. 22.15 and Videoclip 22.10), partially anomalous venous connections to a systemic vein, double aortic arch, and vascular rings can be evaluated from this view. Left superior vena cava to coronary sinus or directly to left atrium with an unroofed coronary sinus are best seen from this view or from a left parasternal window in the parasagittal plane.

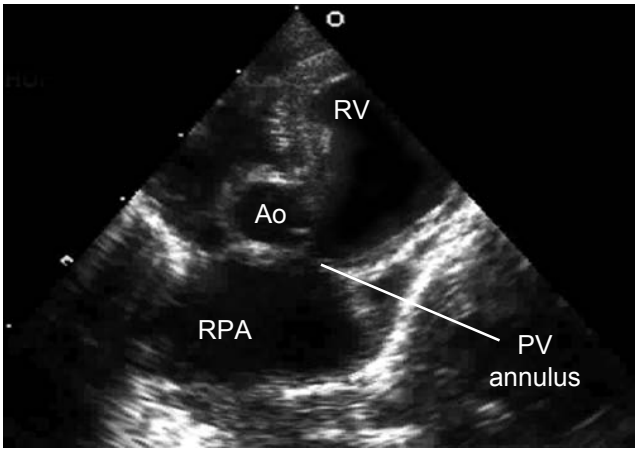

Figure 22.14 Imaging of the branch pulmonary arteries from the left parasternal window in an infant with tetralogy of Fallot and absent pulmonary valve syndrome. Ao, aorta; PV, pulmonary valve; RPA, right pulmonary artery; RV, right ventricle.

Right parasternal view

Imaging from this acoustic window is best performed with the patient in a right decubitus position. This window allows clear imaging of the atrial septum, right superior vena cava, and the right pulmonary veins in right parasternal short-axis, parasagittal and transverse imaging planes. "En face" common AV valve morphology in patients with TOF and common AV canal can also be seen well from this window in short-axis planes.

Preoperative hemodynamic assessment

Color flow mapping and spectral Doppler are crucial in refining the diagnosis, screening for subtle structural abnormalities (e.g., coronary, arch and branch pulmonary artery) and, of course, in assessing the hemodynamics, as described in Chapter 6.

Atrial septum

Color flow mapping of the atrial septum usually demonstrates the left-to-right shunting occurring in TOF even in the presence of severe pulmonary stenosis. Bidirectional or right-to-left shunting may be present in newborns.

Ventricular septal defect

The flow across the large VSD is usually nonrestrictive and bidirectional; as noted above, only rarely is it restrictive. The degree of RV outflow tract obstruction determines the direction of flow across the VSD – less pulmonary stenosis allows predominantly left-to-right shunting, and the clinical scenario of "pink" TOF, even to the point of developing signs and/or symptoms of congestive heart failure. More severe pulmonary stenosis results in predominant right-to-left shunting and the more typical cyanosis. In the typical setting of a nonrestrictive VSD, RV peak pressures cannot exceed systemic levels; right-to-left shunting at the level of the VSD is not synonymous with suprasystemic RV pressures. Suprasystemic RV pressures in TOF can only occur in the setting of a restrictive VSD with pulmonary atresia or severe RV outflow tract obstruction [158]. Also, in the setting of a nonrestrictive malalignment VSD, additional muscular VSDs may be difficult to identify. Therefore, it is essential to interrogate the muscular septum by color flow mapping with a lowered Nyquist limit to identify low-velocity shunting across these small defects (Fig. 22.16 and Videoclip 22.11).

Right ventricular outflow tract and pulmonary arteries

The level of obstruction can be determined by imaging and by sequential pulsed Doppler interrogation starting from within the RV cavity to the pulmonary valve annulus. In severe stenosis, antegrade flow may be demonstrated using a

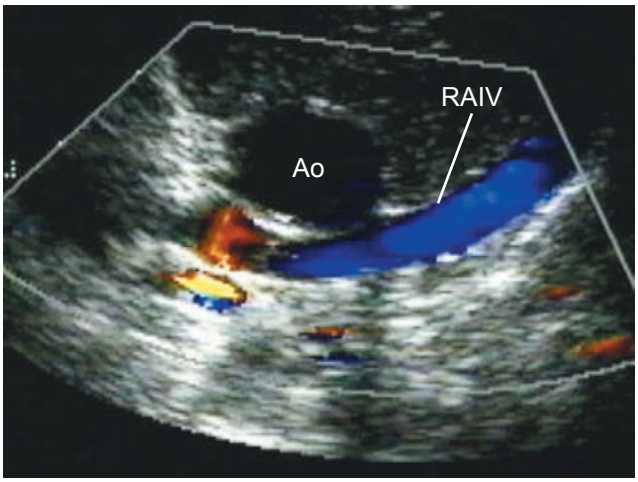

(a)

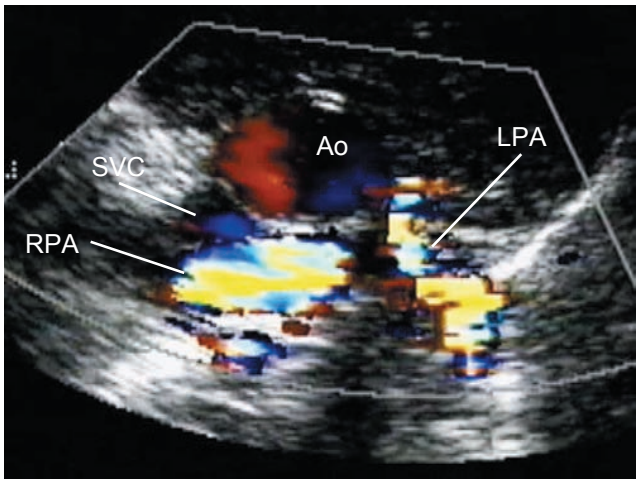

(b)

Figure 22.15 Retroaortic innominate vein (RAIV). **(a)** Imaging from the high left parasternal window in the transverse plane. The left innominate vein is seen posterior to the distal ascending aorta (Ao). **(b)** Inferior tilt of the transducer demonstrates the left (LPA) and right (RPA) pulmonary arteries inferior to the RAIV. SVC, superior vena cava.

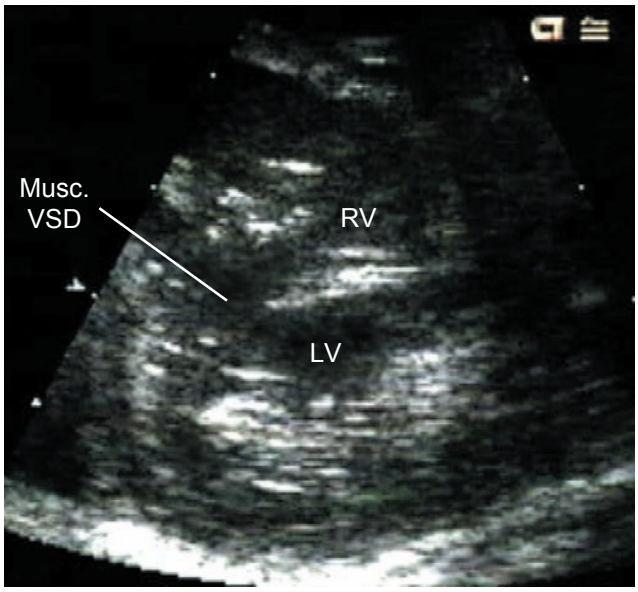

(a)

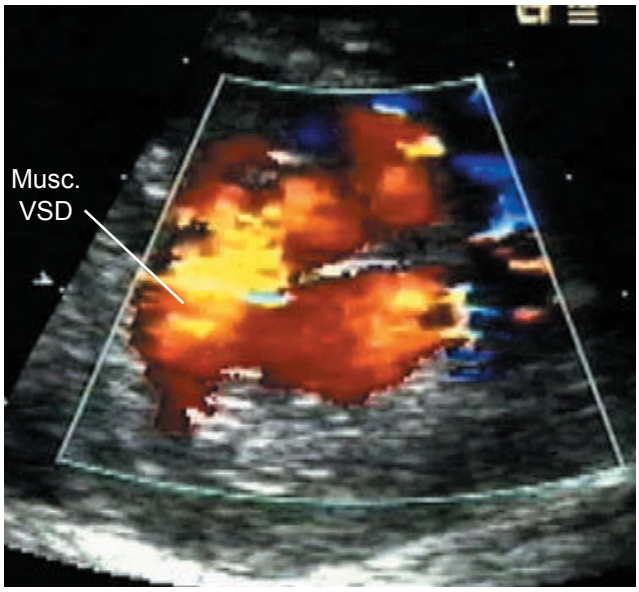

(b)

Figure 22.16 Additional posterior muscular ventricular septal defect (Musc. VSD) seen by 2D imaging **(a)** and by color Doppler with a low Nyquist limit **(b)**. LV, left ventricle; RV, right ventricle.

lower-frequency transducer that achieves a higher Nyquist limit; this allows less "aliasing" of the color flow map of the high-velocity flow across the stenotic outflow tract. Continuous-wave Doppler interrogation is essential to estimate the total maximal instantaneous gradient, but separation of the infundibular and valvar contributions to the total gradient is difficult with any Doppler interrogation technology (Fig. 22.17). The need for transannular patch repair may be predicted in infants weighing less than 10 kg with annular dimension of less than 7 mm [128].

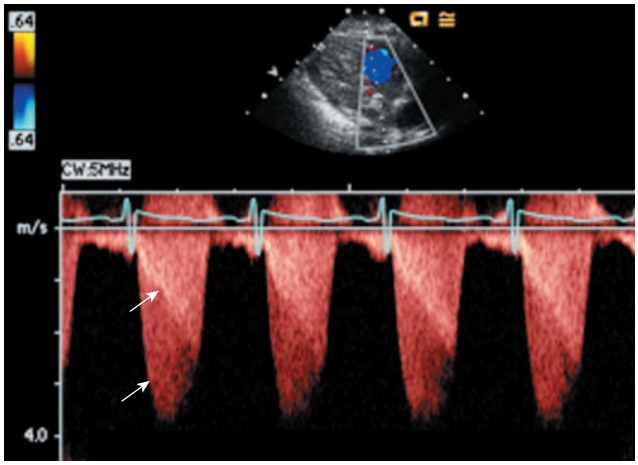

Figure 22.17 Continuous-wave Doppler interrogation of the right ventricular outflow tract and pulmonary valve from the parasternal short-axis view demonstrates high-velocity flow with two velocity profiles. The first arrow points to a late-peaking, dagger-shaped lower-velocity flow profile consistent with dynamic infundibular obstruction, and the second arrow points to a higher velocity profile reflecting the total maximum instantaneous gradient.

In TOF with absent pulmonary valve syndrome, pulmonary insufficiency is easily demonstrated by color flow mapping (Fig. 22.18 and Videoclip 22.12) and may be associated with diastolic flow reversal in the branch pulmonary arteries. In patients with pulmonary atresia, color flow mapping and spectral Doppler interrogation help to identify mediastinal branch pulmonary arteries and collaterals, although color flow mapping may result in false positive diagnosis of aortopulmonary collateral (APC) [103]. In patients with long-segment pulmonary atresia the left atrial appendage can mimic the central main pulmonary artery segment (Videoclip 22.13); this can be further delineated by careful imaging and by demonstration of low velocity to-and-fro flow by color and pulsed-wave Doppler interrogation [161]. Because of its position under the aortic arch, the retroaortic innominate vein (also known as "anomalous brachiocephalic vein") may mimic central confluent branch pulmonary arteries in pulmonary atresia. Doppler interrogation demonstrates the connection of the retroaortic innominate vein to the internal jugular vein or superior vena cava; it can also differentiate the retroaortic innominate vein from a pulmonary artery, by identifying the typical multiphasic venous flow pattern in the innominate vein (Videoclip 22.10).

Atrioventricular valves

Color flow mapping from the apical window is used to assess the AV valve regurgitation that is usually seen in patients with associated malformations of the AV valves (e.g., Ebstein, double-orifice TV and mitral valve [MV], common AV valve

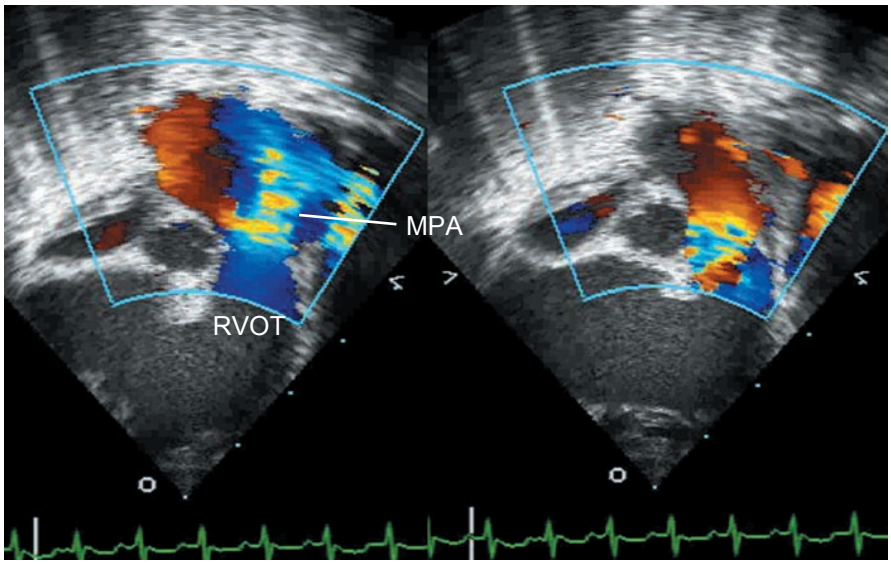

Figure 22.18 Color Doppler flow mapping of the right ventricular outflow tract (RVOT) in an infant with tetralogy of Fallot and absent pulmonary valve syndrome. The left panel shows a systolic frame with antegrade flow from the RVOT to the main pulmonary artery (MPA). The right panel shows a diastolic frame with a wide jet of retrograde flow from the MPA into the RVOT.

and cleft MV). In the setting of significant mitral regurgitation without morphologic abnormalities and/or LV hypokinesis, associated anomalous origin of the LCA from the pulmonary artery must be excluded.

Aortic root dilation and regurgitation

Standard measurements in parasternal views will identify root and ascending aortic dilation, commonly seen in TOF, and allow serial follow-up of aortic size. Aortic regurgitation is uncommon preoperatively; it is most often acquired postoperatively or secondary to endocarditis [141,162].

Coronary arteries

Confirm the coronary origin and branching patterns by high-resolution parasternal imaging, with color flow mapping using a low Nyquist limit to exclude anomalous origin of the left coronary artery from the pulmonary artery. Depressed ventricular function is usually present in the setting of anomalous origin of the left coronary artery from the pulmonary artery (ALCAPA), but if there is associated pulmonary hypertension, as in cases of TOF with minimal pulmonary stenosis or with nonrestrictive patent ductus arteriosus, ventricular function may be normal. Coronary–cameral fistulae may also be detected by color flow mapping but coronary–pulmonary artery fistulae may be obscured by aliased pulmonary artery flow patterns due to the pulmonary stenosis.

Intraoperative and postoperative assessment after TOF repair

Intraoperative echocardiographic assessment of TOF repair is almost always accomplished by using transesophageal echocardiography (TEE) or, in situations where esophageal access is not possible, utilizing an epicardial approach. The goal of the intraoperative TEE evaluation should be aimed at identification of hemodynamically significant lesions that can affect immediate postoperative management as well as long-term outcomes. Knowing the details of the surgical repair is essential to a successful intraoperative echocardiographic evaluation, and good communication between the surgeon and echocardiographer is paramount. Conventional echocardiography and TEE are important in the evaluation of the postoperative patient in the intensive care unit (ICU), especially to assess acute changes in clinical status. In addition to the TEE evaluation described below, conventional echocardiography enables assessment of diaphragmatic motion and pleural or pericardial effusions. Conventional windows are often superior to TEE for assessment of the aortic arch and branch pulmonary arteries.

Evaluation of surgical repair often begins with scanning for residual septal defects. The impact of residual atrial septal defects depends on the relative compliances of the right and left heart chambers. In the setting of RV dysfunction, which is common after TOF repair, right-to-left atrial-level shunting results in postoperative hypoxemia. In this setting, right-to-left diastolic shunting may also be noted across a residual VSD, even in the setting of left-to-right systolic shunting. Small residual VSDs with restrictive flow may have no impact on postoperative hemodynamics. However, intraoperative echocardiographic estimation of Qp:Qs can be challenging; the assessment of hemodynamic significance may be supplemented by direct intraoperative pressure and saturation data. Residual "intramural" VSDs occur when the VSD patch allows the blood to pursue a tortuous course within the myocardial trabeculae before exiting into the RV cavity [163]. These defects are often quite small or inapparent initially, but may enlarge progressively in mid- to long-term follow-up. Occasionally, surgical closure of the large malalignment VSD may unmask previously undiagnosed additional small muscular VSDs.

Evaluation for residual RV outflow tract obstruction can be achieved from deep transgastric longitudinal imaging planes. Pulmonary valve function and branch pulmonary arteries can be evaluated from the mid- and high esophageal imaging planes. Although RV pressures can be estimated from Doppler interrogation of tricuspid regurgitation, residual VSD jets or RV outflow tract gradients, the angle of interrogation is often suboptimal. When possible, such Doppler data should be confirmed by direct measurement of pressures.

It is important to assess tricuspid and aortic valve competence because either valve may be distorted by VSD patch closure. Postoperatively acquired small coronary fistulae are commonly seen following infundibular muscle resection; these hemodynamically insignificant fistulae often regress on follow-up exams but may persist in the long term [86].

Immediate postoperative TEE assessment of biventricular function following separation from cardiopulmonary bypass utilizes deep transgastric short-axis and mid-esophageal axial imaging planes. The functional assessment may be somewhat limited in the presence of arrhythmia or paced rhythm.

Echocardiography in adults with TOF

Unrepaired TOF in adults is rare and adult surgical outcomes are generally good, with in-hospital mortality reported to be as low as 1.9% and significant functional improvement in the survivors [164]. Evaluation of adults is different only in so far as obtaining adequate acoustic access may be more challenging. Otherwise, assessment should proceed as described above.

Late echocardiographic assessment of adolescents and adults with repaired TOF involves additional issues, considered under the following three categories:

1 Assessment of physiologic and hemodynamic parameters that influence outcome [165–168], including (i) RV and LV size and function; (ii) pulmonary regurgitation and/or stenosis; and (iii) tricuspid regurgitation. Similar to the electrophysiologic criteria of QRS duration >180 ms, serious derangements in the above categories have a significant impact on long-term outcomes, risk for ventricular arrhythmias and sudden death.

2 Assessment of anatomic criteria of unknown significance on outcomes: RVOT aneurysm, DCRV, aortic dilation and aortic regurgitation.

3 Assessment of suitability of RVOT morphology for transcatheter pulmonary valve implantation. Based on current criteria, RVOT diameter <22 mm and prior repair without a transannular patch is generally considered suitable for catheter deployment of a stented pulmonary valve [169–171]. However, patients with RVOT diameter somewhat larger than 22 mm have undergone successful percutaneous valve implantation [172].

Assessment of RV function

Systolic function

Assessment of RV size and function is limited to qualitative estimates by 2D echocardiography. Quantitative evaluation by tissue Doppler-derived techniques correlates with CMR-measured RV size and function; CMR is the "gold standard" for RV size and function assessment. Indices derived from Doppler tissue imaging, such as systolic velocities and strain, have been shown to correlate well with CMR-derived RV ejection fraction and can be utilized as an interim follow-up tool [173–175]. Dobutamine stress echocardiography in combination with Doppler tissue indices (DTI) has been used to study RV functional reserve. Increasing the degree of pulmonary regurgitation (PR) has a negative impact on RV functional reserve [176,177]. Decreased systolic and annular E′ DTI velocities correlate with decreasing peak oxygen consumption during exercise. Importantly, RV systolic velocity is predictive of exercise capacity in repaired TOF [178].

Assessment of dyssynchrony may have a role in postoperative TOF evaluation. An increase in interventricular delay of >55 ms has been correlated with increased risk for arrhythmia [173]. Recently, three-dimensional (3D) echo measurements of RV size and function have been correlated with CMR, and this technology needs further evaluation and validation in order to become a reproducible and accurate method for serial assessment of RV size and function [179].

Diastolic function

The presence of antegrade late systolic (during atrial systole) pulmonary artery flow is posited as a sign of RV diastolic dysfunction or reduced compliance.

Assessment of left ventricular function

Accurate quantification of LV function is limited by traditional echocardiographic methods, again because of geometric issues in the postoperative patient. Conventionally derived shortening and ejection fractions are unreliable secondary to nearly universal diastolic septal flattening, which affects the geometric assumptions that underlie the methods used to calculate these ejection phase indices. Furthermore, RV dilation may interfere with apical windows, because the RV apex often replaces the LV apex as the acoustic window. Although theoretically septal flattening should similarly negatively affect LV cross-sectional area change fraction, we have found reasonable correlation between LV cross-sectional area fraction and CMR-derived LV ejection fraction (S. Srivastava and IA Parness, unpublished data). Again, 3D echocardiography, by measuring actual volumes without use of geometric assumptions, should provide accurate serial quantification of volumes and systolic function as long as acoustic windows are adequate. Diastolic LV function indices have not been systematically studied in TOF.

Assessment of pulmonary regurgitation

Echocardiographic evaluation of pulmonary regurgitation (PR) can be assessed by the following criteria:

1 Jet width – PR may be graded according to the ratio of jet width/RV outflow diameter: mild ≤1/3; moderate 1/3–2/3; and severe ≥2/3.

2 Ratio of duration of PR/duration of diastole >0.77 correlates with PR regurgitant fraction >24.5% by CMR [180].

3 Pressure half-time <100 ms correlates with hemodynamically significant PR [172,181].

4 Presence of diastolic flow reversal in branch pulmonary arteries is associated with hemodynamically significant PR [182].

Assessment of pulmonary stenosis

Doppler estimates of RV outflow tract obstruction or peripheral branch pulmonary artery stenosis may be limited by suboptimal angle of interrogation and/or overestimation due to pressure recovery. Appropriate alignment with LPA flow can be achieved from the high right parasternal or suprasternal notch windows; and with the RPA flow from the high left parasternal window. A pattern of continuous antegrade diastolic flow with a "sawtooth" configuration is consistent with branch pulmonary artery stenosis.

Assessment of right atrial size

Assessment of right atrial size is qualitative. Right atrial enlargement is considered a risk factor for arrhythmias, and its size should be evaluated in routine follow-up. Right atrial enlargement in the absence of significant tricuspid insufficiency may signal the presence of restrictive RV physiology.

Assessment of tricuspid regurgitation

Increased RV size due to PR can lead to annular dilation and an increase in tricuspid regurgitation that further aggravates RV volume overload [183]. Tricuspid regurgitation is infrequently a major contributor to RV dilation in postoperative TOF unless there is an associated congenital tricuspid valve anomaly or inadvertent tricuspid valve damage during surgical repair.

Assessment of repaired TOF in pregnancy

Severe PR is associated with an increased incidence of low birth-weight babies, but does not affect maternal and infant morbidity and mortality [184].

Prenatal assessment

Poon et al. reported their experience with fetal diagnosis of TOF at a mean gestational age of 20.6 weeks [31]. Increased nuchal translucency measurement >95th percentile was common (47%) but 19/37 fetuses had normal chromosomes. In their study cohort, 49% had chromosomal anomalies, including the 22q11 microdeletion in 15, with additional extracardiac malformations in 50% and additional cardiac malformations in 57%. In 70/129 (54%) cases, the parents chose termination of pregnancy.

Associated extracardiac anomalies can occur in up to approximately 30% of affected infants and children, and the incidence can be as high as 50–60% in fetal TOF. Important chromosomal and syndromic associations include microdeletion of chromosome 22q11, trisomies 21 and 18, pentalogy of Cantrell, VATER (vertebral anomalies, anal atresia, cardiac anomalies, tracheo-esophageal fistula, esophageal atresia, renal anomalies) or CHARGE (coloboma, heart defects, atresia of the choanae, retardation of growth, genital abnormalities, ear anomalies) association, tracheo-esophageal fistula, and omphalocele. Association with cleft palate may suggest velocardiofacial syndrome [31,185–187]. Appropriate prenatal evaluation and counseling for TOF requires careful high-level screening for noncardiac anomalies and chromosomal anomalies.

The diagnosis of TOF is often not obvious in the 4-chamber view. The LV outflow tract view or the 5-chamber view demonstrate aortic override (Fig. 22.19a and Videoclip 22.14), and on color flow mapping flow is directed from both ventricles into the aorta. The basal short-axis view demonstrates the deviation of the conal septum, malalignment VSD, and subpulmonary stenosis (Fig. 22.19b and Videoclip 22.15(a,b)). The 3-vessel view (high axial cut of the superior vena cava, aorta, and main pulmonary artery) can demonstrate vessel size discrepancy, with the aorta being larger than the pulmonary artery (Fig. 22.19c) [187]. The flow in the ductus arteriosus would be retrograde in case of severe pulmonic stenosis or atresia. Aortic arch sidedness and arch anomalies can be evaluated in the 3-vessel axial view, and the transmission qualities of the unexpanded fetal lungs can facilitate the prenatal diagnosis of vascular rings (Fig. 22.20). Serial prenatal echocardiography is recommended, primarily to reassess for progressive subpulmonary stenosis and/or progressive pulmonary artery hypoplasia.

TOF with pulmonary atresia

Pulmonary atresia with TOF can be valvar, short-segment involving just the valve and proximal main pulmonary artery, or long-segment atresia in which the entire main pulmonary artery segment is missing. With long-segment atresia, it is prognostically essential to determine if there are central confluent mediastinal pulmonary arteries, and if present, their degree of hypoplasia. Pulmonary stenosis can be progressive and evolve prenatally into pulmonary atresia [188,189]. Pulmonary blood supply from multiple aortopulmonary collaterals can be seen prenatally [188,189]. With short-segment pulmonary atresia, hypoplastic branch pulmonary arteries may be supplied by a ductus.

Tetralogy of Fallot with pulmonary atresia may be mistaken for truncus arteriosus if the branch pulmonary artery origins are not clearly demonstrated. Both lesions share

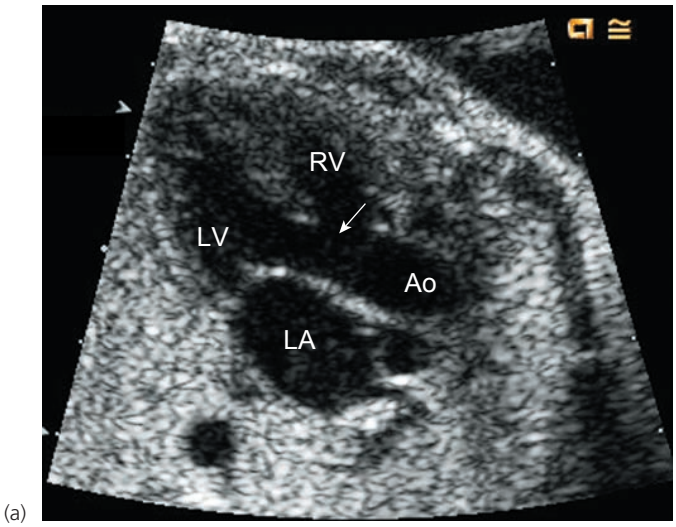

(a)

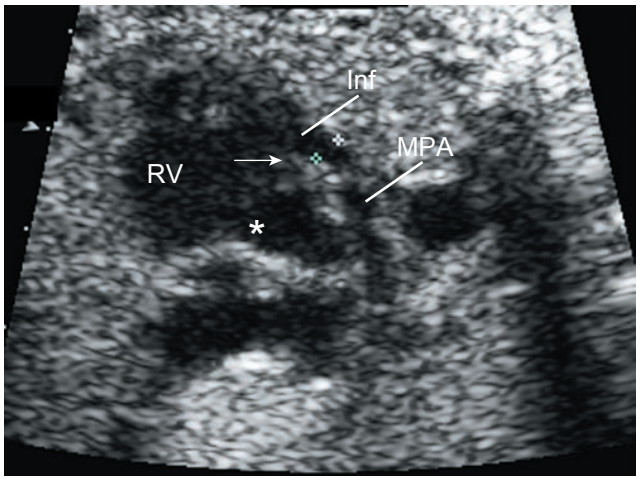

(b)

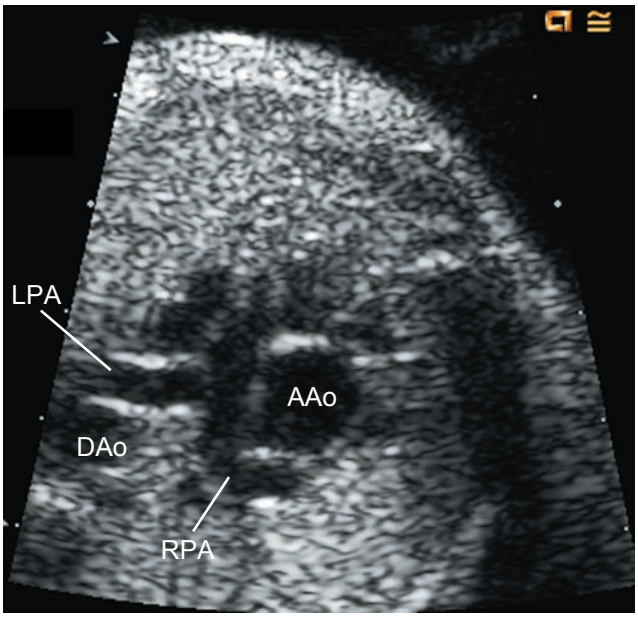

(c)

Figure 22.19 Fetal echocardiography in tetralogy of Fallot with pulmonary stenosis. **(a)** Long-axis view of the left ventricular outflow demonstrates a large aortic root overriding a ventricular septal defect (arrow). **(b)** Imaging of the anteriorly deviated conal septum (arrow) and the conoventricular septal defect (*). Note the hypoplastic infundibulum (Inf) and main pulmonary artery (MPA). **(c)** Transverse view of the fetal chest demonstrating the relatively small branch pulmonary arteries in relation to the dilated ascending aorta (AAo). DAo, descending aorta; LA, left atrium; LPA, left pulmonary artery; LV, left ventricle; RPA, right pulmonary artery; RV, right ventricle.

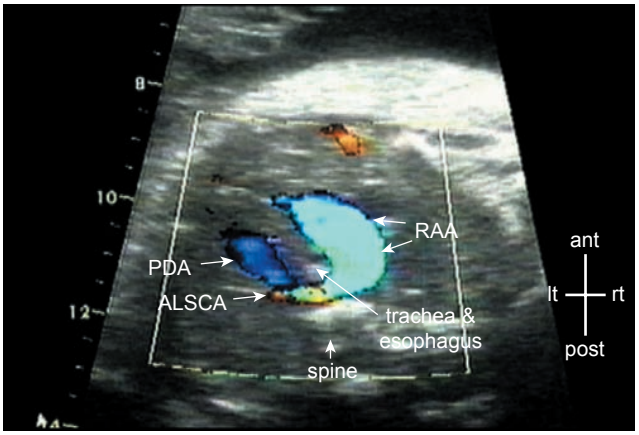

Figure 22.20 Prenatal echocardiographic diagnosis of tetralogy of Fallot with vascular ring. The ring comprises a right aortic arch (RAA), aberrant origin of the left subclavian artery (ALSCA), and left patent ductus arteriosus (PDA). ant, anterior; post, posterior; lt, left; rt, right.

features of a large anterior malalignment VSD with overriding and enlarged semilunar root. Hence it is essential to image the origin or absence of branch pulmonary arteries when only one major vessel is seen overriding a malalignment VSD. It is also important to differentiate from truncus arteriosus the rare association of anomalous origin of a branch pulmonary artery from the ascending aorta with TOF (in the latter case, the contralateral branch pulmonary artery will be supplied by a separate, if small, pulmonary valve).

TOF with absent pulmonary valve

This lesion is easily diagnosed in utero because its key features stand out: the dysplastic pulmonary valve with stenosis and regurgitation and the aneurysmal main and/or branch pulmonary arteries (Fig. 22.21 and Videoclip 22.16(a,b)). The ductus arteriosus is typically absent. Progressive RV and main pulmonary artery dilation may occur and result in hydrops fetalis due to RV dysfunction [118,190,191].

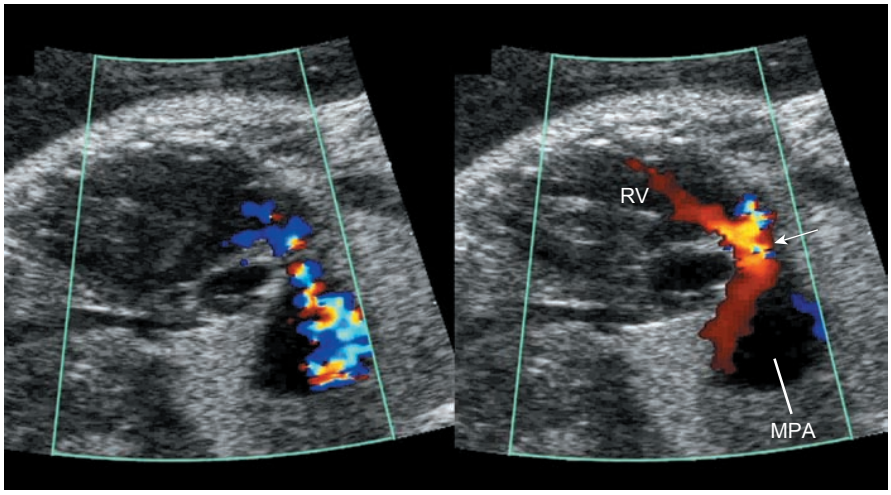

Figure 22.21 Fetal echocardiogram in tetralogy of Fallot with absent pulmonary valve syndrome. The left panel shows a systolic frame with antegrade flow from the right ventricular outflow tract to a markedly dilated main pulmonary artery (MPA). The right panel shows a diastolic frame with pulmonary regurgitation jet into the right ventricle (RV). The arrow points to the location of the dysplastic pulmonary valve.

Neonatal outcome in published series was not predicted by the degree of pulmonary artery dilation but, as expected, outcome was poor in fetuses with fetal hydrops [118].

TOF with complete atrioventricular canal

In this lesion, the 4-chamber view is abnormal because the VSD extends from the inlet to the outlet septum. It is important to determine whether there is a balanced versus unbalanced AV canal defect as well as the degree of any associated AV valve regurgitation.

Serial fetal echocardiographic evaluation is recommended to screen for progression of pulmonary stenosis and/or branch pulmonary artery hypoplasia. Mild pulmonary stenosis in the early second trimester may progress to severe stenosis or atresia by the late third trimester [192]. This impacts upon neonatal management and counseling of the parents. As mentioned above, amniocentesis for associated chromosomal anomalies and fluorescence in situ hybridization (FISH) for microdeletion should be suggested routinely as this also bears a significant impact on neonatal outcome. The association of intrauterine growth retardation, polyhydramnios, increased nuchal translucency, and aortic arch anomalies with TOF can predict 22q11 deletion with a sensitivity of 88% [185,193]. The postnatal prognosis of isolated TOF is good but outcomes of fetal diagnosis of conotruncal anomalies can be poor, mainly due to the frequent association with chromosomal and/or extracardiac anomalies, often leading to intrauterine or early neonatal death [31,194].

References

1. Becker AE, Connor M, Anderson RH. Tetralogy of Fallot: a morphometric and geometric study. *Am J Cardiol* 1975;35:402–12.
2. Van Praagh R, Geva T, Kreutzer J. Ventricular septal defects: how shall we describe, name and classify them? *J Am Coll Cardiol* 1989;14:1298–9.
3. Van Praagh R, Van Praagh S, Nebesar RA et al. Tetralogy of Fallot: underdevelopment of the pulmonary infundibulum and its sequelae. *Am J Cardiol* 1970;26:25–33.
4. Abbott ME, Dawson WT. The clinical classification of congenital cardiac disease, with remarks upon its pathological anatomy, diagnosis and treatment. *Int Clin* 1924;4:156–88.
5. Jacobs ML. Congenital Heart Surgery Nomenclature and Database Project: tetralogy of Fallot. *Ann Thorac Surg* 2000;69 (4 Suppl.):S77–82.
6. Loffredo CA. Epidemiology of cardiovascular malformations: prevalence and risk factors. *Am J MedGenet* 2000;97:319–25.
7. Hoffman JI, Kaplan S. The incidence of congenital heart disease. *J Am Coll Cardiol* 2002;39:1890–900.
8. Castaneda AR, Freed MD, Williams RG, Norwood WI. Repair of tetralogy of Fallot in infancy. Early and late results. *J Thorac Cardiovasc Surg* 1977;74:372–81.
9. Rabinovitch M, Herrera-deLeon V, Castaneda AR, Reid L. Growth and development of the pulmonary vascular bed in patients with tetralogy of Fallot with or without pulmonary atresia. *Circulation* 1981;64:1234–49.
10. Karr SS, Brenner JI, Loffredo C et al. Tetralogy of Fallot. The spectrum of severity in a regional study, 1981–1985. *Am J Dis Child* 1992;146:121–4.
11. Marelli AJ, Mackie AS, Ionescu-Ittu R et al. Congenital heart disease in the general population: changing prevalence and age distribution. *Circulation* 2007;115:163–72.
12. de la Cruz MV, Sanchez Gomez C, Arteaga MM, Arguello C. Experimental study of the development of the truncus and the conus in the chick embryo. *J Anat* 1977;123:661–86.
13. Mjaatvedt CH, Nakaoka T, Moreno-Rodriguez R et al. The outflow tract of the heart is recruited from a novel heart-forming field. *Dev Biol* 2001;238:97–109.
14. Waldo KL, Kumiski DH, Wallis KT et al. Conotruncal myocardium arises from a secondary heart field. *Development* 2001;128:3179–88.
15. Kelly RG. Molecular inroads into the anterior heart field. *Trends Cardiovasc Med* 2005;15:51–6.
16. Ward C, Stadt H, Hutson M, Kirby ML. Ablation of the secondary heart field leads to tetralogy of Fallot and pulmonary atresia. *Dev Biol* 2005;284:72–83.

17. Towbin JA, Belmont J. Molecular determinants of left and right outflow tract obstruction. *Am J Med Genet* 2000;97:297–303.
18. Kelly RG, Brown NA, Buckingham ME. The arterial pole of the mouse heart forms from Fgf10-expressing cells in pharyngeal mesoderm. *Dev Cell* 2001;1:435–40.
19. Kelly RG, Buckingham ME. The anterior heart-forming field: voyage to the arterial pole of the heart. *Trends Genet* 2002; 18:210–16.
20. Bajolle F, Zaffran S, Kelly RG et al. Rotation of the myocardial wall of the outflow tract is implicated in the normal positioning of the great arteries. *Circ Res* 2006;98:421–8.
21. Kirby ML, Gale TF, Stewart DE. Neural crest cells contribute to normal aorticopulmonary septation. *Science* 1983;220:1059–61.
22. Restivo A, Piacentini G, Placidi S et al. Cardiac outflow tract: a review of some embryogenetic aspects of the conotruncal region of the heart. *Anat Rec A Discov Mol Cell Evol Biol* 2006; 288:936–43.
23. Yelbuz TM, Waldo KL, Kumiski DH et al. Shortened outflow tract leads to altered cardiac looping after neural crest ablation. *Circulation* 2002;106:504–10.
24. Tevosian SG, Deconinck AE, Tanaka M et al. FOG-2, a cofactor for GATA transcription factors, is essential for heart morphogenesis and development of coronary vessels from epicardium. *Cell* 2000;101:729–39.
25. Gelb BD. Molecular genetics of congenital heart disease. *Curr Opin Cardiol* 1997;12:321–8.
26. van den Akker NM, Molin DG, Peters PP et al. Tetralogy of Fallot and alterations in vascular endothelial growth factor-A signaling and notch signaling in mouse embryos solely expressing the VEGF120 isoform. *Circ Res* 2007;100:842–9.
27. Pierpont ME, Basson CT, Benson DW Jr et al. Genetic basis for congenital heart defects: current knowledge: a scientific statement from the American Heart Association Congenital Cardiac Defects Committee, Council on Cardiovascular Disease in the Young: endorsed by the American Academy of Pediatrics. *Circulation* 2007;115:3015–38.
28. Michielon G, Marino B, Formigari R et al. Genetic syndromes and outcome after surgical correction of tetralogy of Fallot. *Ann Thorac Surg* 2006;81:968–75.
29. Vergara P, Digilio MC, Zorzi AD et al. Genetic heterogeneity and phenotypic anomalies in children with atrioventricular canal defect and tetralogy of Fallot. *Clin Dysmorphol* 2006;15: 65–70.
30. Marino B, Digilio MC, Grazioli S et al. Associated cardiac anomalies in isolated and syndromic patients with tetralogy of Fallot. *Am J Cardiol* 1996;77:505–8.
31. Poon LC, Huggon IC, Zidere V, Allan LD. Tetralogy of Fallot in the fetus in the current era. *Ultrasound Obstet Gynecol* 2007; 29:625–7.
32. Van Praagh S, Truman T, Firpo A et al. Cardiac malformations in trisomy-18: a study of 41 postmortem cases. *J Am Coll Cardiol* 1989;13:1586–97.
33. Tartaglia M, Gelb BD. Noonan syndrome and related disorders: genetics and pathogenesis. *Annu Rev Genomics Hum Genet* 2005; 6:45–68.
34. Tartaglia M, Pennacchio LA, Zhao C et al. Gain-of-function SOS1 mutations cause a distinctive form of Noonan syndrome. *Nat Genet* 2007;39:75–9.
35. Schubbert S, Zenker M, Rowe SL et al. Germline KRAS mutations cause Noonan syndrome. *Nat Genet* 2006;38:331–6.
36. Roberts AE, Hult B, Rehm HL et al. The PTPN11 gene is not implicated in nonsyndromic hypertrophic cardiomyopathy. *Am J Med Genet A* 2005;132:333–4.
37. Krantz ID. Alagille syndrome: chipping away at the tip of the iceberg. *Am J Med Genet* 2002;112:160–2.
38. McElhinney DB, Krantz ID, Bason L et al. Analysis of cardiovascular phenotype and genotype–phenotype correlation in individuals with a JAG1 mutation and/or Alagille syndrome. *Circulation* 2002;106:2567–74.
39. Bruneau BG, Nemer G, Schmitt JP et al. A murine model of Holt–Oram syndrome defines roles of the T-box transcription factor Tbx5 in cardiogenesis and disease. *Cell* 2001;106: 709–21.
40. Kumar A, Friedman JM, Taylor GP, Patterson MW. Pattern of cardiac malformation in oculoauriculovertebral spectrum. *Am J Med Genet* 1993;46:423–6.
41. Goldmuntz E. DiGeorge syndrome: new insights. *Clin Perinatol* 2005;32:963–78, ix–x.
42. Goldmuntz E, Geiger E, Benson DW. NKX2.5 mutations in patients with tetralogy of fallot. *Circulation* 2001;104:2565–8.
43. McElhinney DB, Clark BJ 3rd, Weinberg PM et al. Association of chromosome 22q11 deletion with isolated anomalies of aortic arch laterality and branching. *J Am Coll Cardiol* 2001;37: 2114–9.
44. McElhinney DB, Geiger E, Blinder J et al. NKX2.5 mutations in patients with congenital heart disease. *J Am Coll Cardiol* 2003; 42:1650–5.
45. Pizzuti A, Sarkozy A, Newton AL et al. Mutations of ZFPM2/FOG2 gene in sporadic cases of tetralogy of Fallot. *Hum Mutat* 2003;22:372–7.
46. Koch R, Levy HL, Matalon R et al. The North American Collaborative Study of Maternal Phenylketonuria. Status report 1993. *Am J Dis Child* 1993;147:1224–30.
47. Levy HL, Guldberg P, Guttler F et al. Congenital heart disease in maternal phenylketonuria: report from the Maternal PKU Collaborative Study. *Pediatr Res* 2001;49:636–42.
48. Feldman GL, Weaver DD, Lovrien EW. The fetal trimethadione syndrome: report of an additional family and further delineation of this syndrome. *Am J Dis Child* 1977;131:1389–92.
49. Nora JJ, Nora AH. Familial risk of congenital heart defect. *Am J Med Genet* 1988;29:231–3.
50. Nora JJ, Nora AH. Update on counseling the family with a first-degree relative with a congenital heart defect. *Am J Med Genet* 1988;29:137–42.
51. Nora JJ, Nora AH. Maternal transmission of congenital heart diseases: new recurrence risk figures and the questions of cytoplasmic inheritance and vulnerability to teratogens. *Am J Cardiol* 1987;59:459–63.
52. Nora JJ, Nora AH. The evolution of specific genetic and environmental counseling in congenital heart diseases. *Circulation* 1978;57:205–13.
53. Nora JJ, Nora AH. Recurrence risks in children having one parent with a congenital heart disease. *Circulation* 1976;53:701–2.
54. Zellers TM, Driscoll DJ, Michels VV. Prevalence of significant congenital heart defects in children of parents with Fallot's tetralogy. *Am J Cardiol* 1990;65:523–6.

55. Calcagni G, Digilio MC, Sarkozy A et al. Familial recurrence of congenital heart disease: an overview and review of the literature. *Eur J Pediatr* 2007;166:111–6.
56. Geva T, Ayres NA, Pac FA, Pignatelli R. Quantitative morphometric analysis of progressive infundibular obstruction in tetralogy of Fallot. A prospective longitudinal echocardiographic study. *Circulation* 1995;92:886–92.
57. Anderson RH, Weinberg PM. The clinical anatomy of tetralogy of fallot. *Cardiol Young* 2005;15(Suppl. 1):38–47.
58. Anderson RH, Becker AE. Etienne-Louis Arthur Fallot and his tetralogy: a new translation of Fallot's summary and a modern reassessment of this anomaly. *Eur J Cardiothorac Surg* 1990;4: 229–32.
59. Oppenheimer-Dekker A, Gittenberger-de Groot AC, Bartelings MM et al. Abnormal architecture of the ventricles in hearts with an overriding aortic valve and a perimembranous ventricular septal defect ("Eisenmenger VSD"). *Int J Cardiol* 1985;9: 341–55.
60. Gatzoulis MA, Soukias N, Ho SY et al. Echocardiographic and morphological correlations in tetralogy of Fallot. *Eur Heart J* 1999;20:221–31.
61. Fukuda T, Suzuki T, Ito T. Clinical and morphologic features of perimembranous ventricular septal defect with overriding of the aorta – the so-called Eisenmenger ventricular septal defect. A study making comparisons with tetralogy of Fallot and perimembranous ventricular defect without aortic overriding. *Cardiol Young* 2000;10:343–52.
62. Van Praagh R, Corwin RD, Dahlquist EH Jr et al. Tetralogy of Fallot with severe left ventricular anomalous attachment of the mitral valve to the ventricular septum. *Am J Cardiol* 1970; 26:93–101.
63. Rosenquist GC, Sweeney LJ, Stemple DR et al. Ventricular septal defect in tetralogy of Fallot. *Am J Cardiol* 1973;31:749–54.
64. Ando M, Takahashi Y, Kikuchi T, Tatsuno K. Tetralogy of Fallot with subarterial ventricular septal defect. *Ann Thorac Surg* 2003;76:1059–64; discussion 1064–5.
65. Fu YC, Hwang B, Weng ZC et al. Influence of ventricular septal defect type on surgical results in children with tetralogy of Fallot. *Zhonghua Yi Xue Za Zhi (Taipei)* 2000;63:792–7.
66. Capelli H, Somerville J. Atypical Fallot's tetralogy with doubly committed subarterial ventricular septal defect. Diagnostic value of 2-dimensional echocardiography. *Am J Cardiol* 1983; 51:282–5.
67. Vargas FJ, Kreutzer GO, Pedrini M et al. Tetralogy of Fallot with subarterial ventricular septal defect. Diagnostic and surgical considerations. *J Thorac Cardiovasc Surg* 1986;92:908–12.
68. Flanagan MF, Foran RB, Van Praagh R et al. Tetralogy of Fallot with obstruction of the ventricular septal defect: spectrum of echocardiographic findings. *J Am Coll Cardiol* 1988;11:386–95.
69. Faggian G, Frescura C, Thiene G et al. Accessory tricuspid valve tissue causing obstruction of the ventricular septal defect in tetralogy of Fallot. *Br Heart J* 1983;49:324–27.
70. Kumar PR, Rakshak AD, Rajagopal P et al. Tetralogy of Fallot with flap valve ventricular septal defect producing suprasystemic right ventricular pressure: echocardiographic observations. *Indian Heart J* 1998;50:446–50.
71. Tewari P, Mittal P. Accessory tricuspid valve tissue in tetralogy of fallot causes hemodynamic changes during intermittent positive-pressure ventilation. *J Cardiothorac Vasc Anesth* 2006; 20:856–8.
72. van Meurs-van Woezik H, van Suylen RJ, Klein HW. A case of tetralogy of Fallot with pulmonary atresia and restrictive perimembranous ventricular septal defect. *Thorac Cardiovasc Surg* 1997;45:46–7.
73. Davido A, Maarek M, Jullien JL, Corone P. Ebstein's disease associated with Fallot's tetralogy. Apropos of a familial case, review of the literature, embryologic and genetic implications. *Arch Mal Coeur Vaiss* 1985;78:752–6.
74. Delius RE, Kumar RV, Elliott MJ et al. Atrioventricular septal defect and tetralogy of Fallot: a 15-year experience. *Eur J Cardiothorac Surg* 1997;12:171–6.
75. Suzuki K, Ho SY, Anderson RH et al. Morphometric analysis of atrioventricular septal defect with common valve orifice. *J Am Coll Cardiol* 1998;31:217–23.
76. Kaur A, Srivastava S, Lytrivi ID et al. Echocardiographic evaluation and surgical implications of common atrioventricular canal defects with absent or diminutive ostium primum defect. *Am J Cardiol* 2008;101:1648–51.
77. Need LR, Powell AJ, del Nido P, Geva T. Coronary echocardiography in tetralogy of fallot: diagnostic accuracy, resource utilization and surgical implications over 13 years. *J Am Coll Cardiol* 2000;36:1371–7.
78. Chiu IS, Wu CS, Wang JK et al. Influence of aortopulmonary rotation on the anomalous coronary artery pattern in tetralogy of Fallot. *Am J Cardiol* 2000;85:780–4, A9.
79. Johnston TA, Dyer K, Armstrong BA, Bengur AR. Anomalous origin of the left coronary artery in tetralogy of Fallot associated with abnormal mitral valve pathology. *Pediatr Cardiol* 1999;20: 438–40.
80. Carretero J, Rissech M, Mortera C et al. Aortic origin of the left pulmonary artery in an infant with Fallot's tetralogy. *Rev Esp Cardiol* 2005;58:1124–6.
81. Shiraishi I, Yamagishi M, Toiyama K et al. Coronary artery obstruction due to membranous ridge of the right sinus valsalva associated with tetralogy of Fallot: syncope mimics anoxic spell. *Ann Thorac Surg* 2004;77:321–2.
82. Meng CC, Eckner FA, Lev M. Coronary artery distribution in tetralogy of Fallot. *Arch Surg* 1965;90:363–6.
83. Krongrad E, Ritter DG, Hawe A et al. Pulmonary atresia or severe stenosis and coronary artery-to-pulmonary artery fistula. *Circulation* 1972;46:1005–12.
84. Suzuki K, Matsui M, Nakamura Y et al. A case of coronary artery-pulmonary artery fistula in tetralogy of Fallot with pulmonary atresia and major aortopulmonary collateral arteries (MAPCA). *Nippon Kyobu Geka Gakkai Zasshi* 1992;40:2252–7.
85. Sanders SP, Parness IA, Colan SD. Recognition of abnormal connections of coronary arteries with the use of Doppler color flow mapping. *J Am Coll Cardiol* 1989;13:922–6.
86. Chiu SN, Wu MH, Lin MT et al. Acquired coronary artery fistula after open heart surgery for congenital heart disease. *Int J Cardiol* 2005;103:187–92.
87. Edwards WD. Double-outlet right ventricle and tetralogy of Fallot. Two distinct but not mutually exclusive entities. *J Thorac Cardiovasc Surg* 1981;82:418–22.
88. Lev M, Eckner FA. The pathologic anatomy of tetralogy of Fallot and its variations. *Dis Chest* 1964;45:251–61.

89. Cicini MP, Giannico S, Marino B et al. "Acquired" subvalvular aortic stenosis after repair of a ventricular septal defect. *Chest* 1992;101:115–8.
90. Moran AM, Hornberger LK, Jonas RA, Keane JF. Development of a double-chambered right ventricle after repair of tetralogy of Fallot. *J Am Coll Cardiol* 1998;31:1127–33.
91. Wong PC, Sanders SP, Jonas RA et al. Pulmonary valve-moderator band distance and association with development of double-chambered right ventricle. *Am J Cardiol* 1991;68: 1681–6.
92. Galiuto L, O'Leary PW, Seward JB. Double-chambered right ventricle: echocardiographic features. *J Am Soc Echocardiogr* 1996;9:300–5.
93. Juffe Stein A, Kirklin JW. Double chambered right ventricle. Surgical results in 47 cases. *Rev Esp Cardiol* 1981;34:259–63.
94. McElhinney DB, Chatterjee KM, Reddy VM. Double-chambered right ventricle presenting in adulthood. *Ann Thorac Surg* 2000;70:124–7.
95. Morhy Borges Leal S, Andrade JL, de Souza M et al. Anomalous subaortic course of the left brachiocephalic (innominate) vein: echocardiographic diagnosis and report of an unusual association. *Cardiol Young* 2002;12:159–63.
96. Wang JK, Wu MH, Chang CI et al. Malalignment-type ventricular septal defect in double-chambered right ventricle. *Am J Cardiol* 1996;77:839–42.
97. Collett RW, Edwards JE. Persistent truncus arteriosus. A classification according to anatomic subtypes. *Surg Clin North Am* 1949;29:1245.
98. Van Praagh R, Van Praagh S. The anatomy of common aorticopulmonary trunk (truncus arteriosus communis) and its embryologic implications. A study of 57 necropsy cases. *Am J Cardiol* 1965;16:406–25.
99. Bharati S, Paul MH, Idriss FS et al. The surgical anatomy of pulmonary atresia with ventricular septal defect: pseudotruncus. *J Thorac Cardiovasc Surg* 1975;69:713–21.
100. Tchervenkov CI, Roy N. Congenital Heart Surgery Nomenclature and Database Project: pulmonary atresia – ventricular septal defect. *Ann Thorac Surg* 2000;69(4 Suppl.):S97–105.
101. Macartney F, Deverall P, Scott O. Haemodynamic characteristics of systemic arterial blood supply to the lungs. *Br Heart J* 1973;35:28–37.
102. Mackie AS, Gauvreau K, Perry SB et al. Echocardiographic predictors of aortopulmonary collaterals in infants with tetralogy of fallot and pulmonary atresia. *J Am Coll Cardiol* 2003;41:852–7.
103. Acherman RJ, Smallhorn JF, Freedom RM. Echocardiographic assessment of pulmonary blood supply in patients with pulmonary atresia and ventricular septal defect. *J Am Coll Cardiol* 1996;28:1308–13.
104. Hadjo A, Jimenez M, Baudet E et al. Review of the long-term course of 52 patients with pulmonary atresia and ventricular septal defect. Anatomical and surgical considerations. *Eur Heart J* 1995;16:1668–74.
105. Thiene G, Frescura C, Bortolotti U et al. The systemic pulmonary circulation in pulmonary atresia with ventricular septal defect: concept of reciprocal development of the fourth and sixth aortic arches. *Am Heart J* 1981;101:339–44.
106. Nakata S, Imai Y, Takanashi Y et al. A new method for the quantitative standardization of cross-sectional areas of the pulmonary arteries in congenital heart diseases with decreased pulmonary blood flow. *J Thorac Cardiovasc Surg* 1984;88:610–9.
107. Shinonaga M, Miyamura H, Watanabe H et al. Tetralogy of Fallot with a restrictive ventricular septal defect caused by a membranous flap. *Nippon Kyobu Geka Gakkai Zasshi* 1994;42:1378–81.
108. Padmanabhan J, Varghese PJ, Lloyd S, Haller JA Jr. Tetralogy of Fallot with suprasystemic pressure in the right ventricle. A case report and review of the literature. *Am Heart J* 1971;82: 805–11.
109. Alborino D, Guccione P, Di Donato R, Marino B. Aortopulmonary window coexisting with tetralogy of Fallot. *J Cardiovasc Surg (Torino)* 2001;42:197–9.
110. Ito M, Kikuchi S, Hachiro Y, Abe T. Anomalous subaortic position of the brachiocephalic vein associated with tetralogy of Fallot. *Ann Thorac Cardiovasc Surg* 2001;7:106–8.
111. Ramaswamy P, Lytrivi ID, Thanjan MT et al. Frequency of aberrant subclavian artery, arch laterality, and associated intracardiac anomalies detected by echocardiography. *Am J Cardiol* 2008;101:677–82.
112. Uretzky G, Puga FJ, Danielson GK et al. Complete atrioventricular canal associated with tetralogy of Fallot. Morphologic and surgical considerations. *J Thorac Cardiovasc Surg* 1984;87: 756–66.
113. Van Praagh S, Porras D, Oppido G et al. Cleft mitral valve without ostium primum defect: anatomic data and surgical considerations based on 41 cases. *Ann Thorac Surg* 2003;75:1752–62.
114. Rao BN, Anderson RC, Edwards JE. Anatomic variations in the tetralogy of Fallot. *Am Heart J* 1971;81:361–71.
115. Jekel L, Benatar A, Bennink GB et al. Tetralogy of Fallot with absent pulmonary valve. A continuing challenge. *Scand Cardiovasc J* 1998;32:213–7.
116. Emmanoulides GC, Thanopoulos B, Siassi B, Fishbein M. "Agenesis" of ductus arteriosus associated with the syndrome of tetralogy of Fallot and absent pulmonary valve. *Am J Cardiol* 1976;37:403–9.
117. Lakier JB, Stanger P, Heymann MA et al. Tetralogy of Fallot with absent pulmonary valve. Natural history and hemodynamic considerations. *Circulation* 1974;50:167–75.
118. Moon-Grady AJ, Tacy TA, Brook MM et al. Value of clinical and echocardiographic features in predicting outcome in the fetus, infant, and child with tetralogy of Fallot with absent pulmonary valve complex. *Am J Cardiol* 2002;89:1280–5.
119. Craatz S, Kunzel E, Spanel-Borowski K. Right-sided aortic arch and tetralogy of Fallot in humans – a morphological study of 10 cases. *Cardiovasc Pathol* 2003;12:226–32.
120. Allen HD, Adams FH, Moss AJ. *Moss and Adams' Heart Disease in Infants, Children, and Adolescents: Including the Fetus and Young Adult*, 6th edn. Philadelphia, PA/New York: Lippincott Williams & Wilkins, 2001.
121. Donti A, Soavi N, Sabbatani P, Picchio FM. Persistent left fifth aortic arch associated with tetralogy of Fallot. *Pediatr Cardiol* 1997;18:229–31.
122. Emmel M, Schmidt B, Schickendantz S. Double aortic arch in a patient with Fallot's tetralogy. *Cardiol Young* 2005;15:52–3.
123. Chen MR, Yu CH. Subclavian and pulmonary steal phenomenon in isolated left subclavian artery with left lung agenesis. *Jpn Heart J* 2002;43:429–32.
124. Krishnan KG, Theodore S, Kiran S, Neelakandhan KS. Embryologic and surgical considerations in tetralogy of Fallot

with right arch and aberrant left subclavian artery from the ascending aorta. *J Thorac Cardiovasc Surg* 2005;130:215–6.
125. Carano N, Piazza P, Agnetti A, Squarcia U. Congenital pulmonary steal phenomenon associated with tetralogy of Fallot, right aortic arch, and isolation of the left subclavian artery. *Pediatr Cardiol* 1997;18:57–60.
126. Yeh CN, Wang JN, Yao CT et al. Isolation of the left subclavian artery in a child with tetralogy of Fallot and right aortic arch. *J Formos Med Assoc* 2005;104:418–20.
127. Soylu M, Demir AD, Tikiz H et al. Left hemitruncus associated with tetralogy of fallot: a case report. *Catheter CardiovascInterv* 2000;51:58–60.
128. Calder AL, Barratt-Boyes BG, Brandt PW, Neutze JM. Postoperative evaluation of patients with tetralogy of Fallot repaired in infancy. Including criteria for use of outflow patching and radiologic assessment of pulmonary regurgitation. *J Thorac Cardiovasc Surg* 1979;77:704–20.
129. Chaturvedi R, Mikailian H, Freedom RM. Crossed pulmonary arteries in tetralogy of Fallot. *Cardiol Young* 2005;15:537.
130. Castaneda AR, Kirklin JW. Tetralogy of Fallot with aorticopulmonary window. Report of two surgical cases. *J Thorac Cardiovasc Surg* 1977;74:467–8.
131. Dipchand AI, Giuffre M, Freedom RM. Tetralogy of Fallot with non-confluent pulmonary arteries and aortopulmonary septal defect. *Cardiol Young* 1999;9:75–7.
132. Takeda Y, Asou T, Fakhri D et al. Pulmonary artery sling associated with tetralogy of fallot. *Asian Cardiovasc Thorac Ann* 2005;13:77–8.
133. Calder AL, Brandt PW, Barratt-Boyes BG, Neutze JM. Variant of tetralogy of fallot with absent pulmonary valve leaflets and origin of one pulmonary artery from the ascending aorta. *Am J Cardiol* 1980;46:106–16.
134. Recto MR, Parness IA, Gelb BD et al. Clinical implications and possible association of malposition of the branch pulmonary arteries with DiGeorge syndrome and microdeletion of chromosomal region 22q11. *Am J Cardiol* 1997;80:1624–7.
135. Zimmerman FJ, Berdusis K, Wright KL, Alboliras ET. Echocardiographic diagnosis of anomalous origins of the pulmonary arteries from the pulmonary trunk (crossed pulmonary arteries). *Am Heart J* 1997;133:257–60.
136. Siwik ES, Everman D, Morrison S. Images in cardiology: Crossed pulmonary arteries, ventricular septal defect, and chromosome 22q11 deletion. *Heart* 2002;88:88.
137. Hohn AR, Jain KK, Tamer DM. Supravalvular mitral stenosis in a patient with tetralogy of Fallot. *Am J Cardiol* 1968;22:733–7.
138. Aru GM, Juraszek A, Moskowitz I, Van Praagh R. Tetralogy of Fallot with congenital aortic valvar stenosis: the tetralogy-truncus interrelationship. *Pediatr Cardiol* 2006;27:354–9.
139. Freedom RM, Benson LN, Mikailian H. Aortic coarctation in an infant with tetralogy and pulmonary atresia. *Cardiol Young* 2005;15:667–8.
140. Ermis C, Gupta-Malhotra M, Titus JL. An obstructive bicuspid aortic valve in the setting of tetralogy of Fallot with pulmonary atresia: a rare combination. *Cardiol Young* 2004;14:99–101.
141. Capelli H, Ross D, Somerville J. Aortic regurgitation in tetrad of Fallot and pulmonary atresia. *Am J Cardiol* 1982;49:1979–83.
142. Alayunt A, Yagdi T, Alat I et al. Left ventricular diverticulum associated with Cantrell's syndrome and tetralogy of Fallot in an adult. *Scand Cardiovasc J* 2001;35:55–7.
143. Van Praagh R, Corsini I. Cor triatriatum: pathologic anatomy and a consideration of morphogenesis based on 13 postmortem cases and a study of normal development of the pulmonary vein and atrial septum in 83 human embryos. *Am Heart J* 1969;78:379–405.
144. Carroll SJ, Solowiejczyk D, Gersony WM. Preoperative diagnosis of co-existing divided left atrium and tetralogy of Fallot. *Cardiol Young* 2004;14:456–9.
145. Bittmann S, Ulus H, Springer A. Combined pentalogy of Cantrell with tetralogy of Fallot, gallbladder agenesis, and polysplenia: a case report. *J Pediatr Surg* 2004;39:107–9.
146. Santini F, Jonas RA, Sanders SP, Van Praagh R. Tetralogy of Fallot [S,D,I]: successful repair without a conduit. *Ann Thorac Surg* 1995;59:747–9.
147. Van Praagh R. Tetralogy of Fallot [S,D,I]: a recently discovered malformation and its surgical management. *Ann Thorac Surg* 1995;60:1163–5.
148. Foran RB, Belcourt C, Nanton MA et al. Isolated infundibuloarterial inversion (S,D,I): a newly recognized form of congenital heart disease. *Am Heart J* 1988;116:1337–50.
149. Ferrin LM, Atik E, Aiello V et al. Tetralogy of Fallot associated with left atrial isomerism. *Arq Bras Cardiol* 1996;67:249–53.
150. Da Cruz E, Milella L, Corno A. Left isomerism with tetralogy of Fallot and anomalous systemic and pulmonary venous connections. *Cardiol Young* 1998;8:131–3.
151. Fujiwara K, Naito Y, Komai H et al. Tetralogy of Fallot with levoatrial cardinal vein. *Pediatr Cardiol* 1999;20:136–8.
152. Brzezinski M, Keller R, Grichnik KP, Swaminathan M. Persistent left superior vena cava in a patient with a history of tetralogy of Fallot. *Anesth Analg* 2005;100:1269–70.
153. Redington AN, Raine J, Shinebourne EA, Rigby ML. Tetralogy of Fallot with anomalous pulmonary venous connections: a rare but clinically important association. *Br Heart J* 1990;64:325–8.
154. Azhari N, Al-Fadley F, Bulbul ZR. Tetralogy of Fallot associated with scimitar syndrome. *Cardiol Young* 2000;10:70–2.
155. Quaegebeur J, Kirklin JW, Pacifico AD, Bargeron LM Jr. Surgical experience with unroofed coronary sinus. *Ann Thorac Surg* 1979;27:418–25.
156. Oppido G, Napoleone CP, Ragni L et al. Double orifice tricuspid valve in an infant with tetralogy of Fallot. *Ann Thorac Surg* 2006;81:1121–3.
157. Cantrell JR, Haller JA, Ravitch MM. A syndrome of congenital defects involving the abdominal wall, sternum, diaphragm, pericardium, and heart. *Surg Gynecol Obstet* 1958;107:602–14.
158. Musewe NN, Smallhorn JF, Moes CA et al. Echocardiographic evaluation of obstructive mechanism of tetralogy of Fallot with restrictive ventricular septal defect. *Am J Cardiol* 1988;61:664–8.
159. Sanders SP, Bierman FZ, Williams RG. Conotruncal malformations: diagnosis in infancy using subxiphoid 2-dimensional echocardiography. *Am J Cardiol* 1982;50:1361–7.
160. Marino B, Ballerini L, Marcelletti C et al. Right oblique subxiphoid view for two-dimensional echocardiographic visualization of the right ventricle in congenital heart disease. *Am J Cardiol* 1984;54:1064–8.
161. Ramaswamy P, Lytrivi ID, Srivastava S et al. Left atrial appendage: variations in morphology and position causing pitfalls in pediatric echocardiographic diagnosis. *J Am Soc Echocardiogr* 2007;20:1011–6.

162. Niwa K. Aortic root dilatation in tetralogy of Fallot long-term after repair – histology of the aorta in tetralogy of Fallot: evidence of intrinsic aortopathy. *Int J Cardiol* 2005;103:117–9.
163. Preminger TJ, Sanders SP, van der Velde ME et al. "Intramural" residual interventricular defects after repair of conotruncal malformations. *Circulation* 1994;89:236–42.
164. Ghavidel AA, Javadpour H, Tabatabaei MB et al. Complete surgical repair of tetralogy of Fallot in adults, is it ever too late? *J Card Surg* 2008;23:23–6.
165. Gatzoulis MA, Elliott JT, Guru V et al. Right and left ventricular systolic function late after repair of tetralogy of Fallot. *Am J Cardiol* 2000;86:1352–7.
166. Geva T. Indications and timing of pulmonary valve replacement after tetralogy of Fallot repair. *Semin Thorac Cardiovasc Surg Pediatr Card Surg Annu* 2006:11–22.
167. Knauth AL, Gauvreau K, Powell A et al. Ventricular size and function assessed by cardiac MRI predict major adverse clinical outcomes late after tetralogy of Fallot repair. *Heart* 2008;94: 211–6.
168. Knauth AL, Gauvreau K, Powell AJ et al. Ventricular size and function assessed by cardiac MRI predict major adverse clinical outcomes late after tetralogy of Fallot repair. *Heart* 2008;94: 211–6.
169. Lurz P, Coats L, Khambadkone S et al. Percutaneous pulmonary valve implantation: impact of evolving technology and learning curve on clinical outcome. *Circulation* 2008;117: 1964–72.
170. Schievano S, Coats L, Migliavacca F et al. Variations in right ventricular outflow tract morphology following repair of congenital heart disease: implications for percutaneous pulmonary valve implantation. *J Cardiovasc Magn Reson* 2007;9:687–95.
171. Schievano S, Migliavacca F, Coats L et al. Percutaneous pulmonary valve implantation based on rapid prototyping of right ventricular outflow tract and pulmonary trunk from MR data. *Radiology* 2007;242:490–7.
172. Schreiber C, Horer J, Vogt M et al. A new treatment option for pulmonary valvar insufficiency: first experiences with implantation of a self-expanding stented valve without use of cardiopulmonary bypass. *Eur J Cardiothorac Surg* 2007;31:26–30.
173. D'Andrea A, Caso P, Sarubbi B et al. Right ventricular myocardial activation delay in adult patients with right bundle branch block late after repair of Tetralogy of Fallot. *Eur J Echocardiogr* 2004;5:123–31.
174. Lytrivi ID, Lai WW, Ko HH et al. Color Doppler tissue imaging for evaluation of right ventricular systolic function in patients with congenital heart disease. *J Am Soc Echocardiogr* 2005;18: 1099–104.
175. Abd El Rahman MY, Hui W, Yigitbasi M et al. Detection of left ventricular asynchrony in patients with right bundle branch block after repair of tetralogy of Fallot using tissue-Doppler imaging-derived strain. *J Am Coll Cardiol* 2005;45:915–21.
176. Baspinar O, Alehan D. Dobutamine stress echocardiography in the evaluation of cardiac haemodynamics after repair of tetralogy of Fallot in children: negative effects of pulmonary regurgitation. *Acta Cardiol* 2006;61:279–83.
177. Apostolopoulou SC, Laskari CV, Tsoutsinos A, Rammos S. Doppler tissue imaging evaluation of right ventricular function at rest and during dobutamine infusion in patients after repair of tetralogy of Fallot. *Int J Cardiovasc Imaging* 2007;23:25–31.
178. Sutton NJ, Peng L, Lock JE et al. Effect of pulmonary artery angioplasty on exercise function after repair of tetralogy of Fallot. *Am Heart J* 2008;155:182–6.
179. Niemann PS, Pinho L, Balbach T et al. Anatomically oriented right ventricular volume measurements with dynamic three-dimensional echocardiography validated by 3-Tesla magnetic resonance imaging. *J Am Coll Cardiol* 2007;50:1668–76.
180. Li W, Davlouros PA, Kilner PJ et al. Doppler-echocardiographic assessment of pulmonary regurgitation in adults with repaired tetralogy of Fallot: comparison with cardiovascular magnetic resonance imaging. *Am Heart J* 2004;147:165–72.
181. Silversides CK, Veldtman GR, Crossin J et al. Pressure half-time predicts hemodynamically significant pulmonary regurgitation in adult patients with repaired tetralogy of fallot. *J Am Soc Echocardiogr* 2003;16:1057–62.
182. Grothoff M, Spors B, Abdul-Khaliq H, Gutberlet M. Evaluation of postoperative pulmonary regurgitation after surgical repair of tetralogy of Fallot: comparison between Doppler echocardiography and MR velocity mapping. *Pediatr Radiol* 2008;38:186–91.
183. Mahle WT, Parks WJ, Fyfe DA, Sallee D. Tricuspid regurgitation in patients with repaired Tetralogy of Fallot and its relation to right ventricular dilatation. *Am J Cardiol* 2003;92:643–5.
184. Gelson E, Gatzoulis M, Steer PJ et al. Tetralogy of Fallot: maternal and neonatal outcomes. *BJOG-Int J Obstet Gy* 2008; 115:398–402.
185. Boudjemline Y, Fermont L, Le Bidois J et al. Can we predict 22q11 status of fetuses with tetralogy of Fallot? *Prenat Diagn* 2002;22:231–4.
186. Chaoui R, Kalache KD, Heling KS et al. Absent or hypoplastic thymus on ultrasound: a marker for deletion 22q11.2 in fetal cardiac defects. *Ultrasound Obstet Gynecol* 2002;20:546–52.
187. Yoo SJ, Lee YH, Kim ES et al. Three-vessel view of the fetal upper mediastinum: an easy means of detecting abnormalities of the ventricular outflow tracts and great arteries during obstetric screening. *Ultrasound Obstet Gynecol* 1997;9:173–82.
188. Miyashita S, Chiba Y. Prenatal demonstration of major aortopulmonary collateral arteries with tetralogy of Fallot and pulmonary atresia. *Fetal Diagn Ther* 2004;19:100–5.
189. Azancot A, Eydoux P, Vuillard E et al. Clinical spectrum of prenatal tetralogy of Fallot. *Arch Mal Coeur Vaiss* 2000;93:587–93.
190. Berg C, Thomsen Y, Geipel A et al. Reversed end-diastolic flow in the umbilical artery at 10–14 weeks of gestation is associated with absent pulmonary valve syndrome. *Ultrasound Obstet Gynecol* 2007;30:254–8.
191. Galindo A, Gutierrez-Larraya F, Martinez JM et al. Prenatal diagnosis and outcome for fetuses with congenital absence of the pulmonary valve. *Ultrasound Obstet Gynecol* 2006;28:32–9.
192. Hornberger LK, Sanders SP, Sahn DJ et al. In utero pulmonary artery and aortic growth and potential for progression of pulmonary outflow tract obstruction in tetralogy of Fallot. *J Am Coll Cardiol* 1995;25:739–45.
193. Boudjemline Y, Fermont L, Le Bidois J et al. Prenatal diagnosis of conotruncal heart diseases. Results in 337 cases. *Arch Mal Coeur Vaiss* 2000;93:583–6.
194. Paladini D, Rustico M, Todros T et al. Conotruncal anomalies in prenatal life. *Ultrasound Obstet Gynecol* 1996;8:241–6.